# End-On Versus Side-On Bonding of Dinitrogen to Dinuclear Early Transition-Metal Complexes

**Michael D. Fryzuk,*,† T. S. Haddad, Murugesapillai Mylvaganam, David H. McConville,‡ and Steven J. Rettig§**

*Contribution from the Department of Chemistry, University of British Columbia, 2036 Main Mall, Vancouver, B.C. Canada V6T 1Z1*

*Received August 18, 1992*

**Abstract:** The preparation of a series of dinuclear complexes of zirconium and tantalum is presented in an effort to determine factors involved in the coordination mode of the bridging dinitrogen ligand. Reduction of $ZrCl_3[N(SiMe_2CH_2PR_2)_2]$ (R = $Pr^i$ and $Bu^t$) with Na/Hg under $N_2$ generates the corresponding dinitrogen complexes $\{[(R_2PCH_2SiMe_2)_2N]ZrCl\}_2(\mu\text{-}\eta^2\text{:}\eta^2\text{-}N_2)$; the X-ray crystal structure of the dark blue derivative having R = $Pr^i$ shows that the dinitrogen unit is bridging in a planar, side-on bonding mode. The N–N bond distance is 1.548(7) Å, which is the longest such distance for any dinitrogen complex reported. Molecular orbital calculations on this molecule indicate that the $N_2$ unit bonds in a side-on fashion due to the unavailability of one of the d orbitals on each zirconium that would normally be involved in a $\pi$-bond with the antibonding $\pi^*$-orbitals of the $N_2$ moiety. This particular zirconium d orbital is unavailable due to the ancillary tridentate ligand which positions the amide donor (and the chloride) to overlap effectively with this d orbital. The results of this MO study also show that the HOMO has $\delta$-symmetry. When the related derivative $Zr(\eta^5\text{-}C_5H_5)Cl_2[N(SiMe_2CH_2PPr^i_2)_2]$ is reduced under $N_2$, the corresponding dinuclear derivative $\{[(Pr^i_2PCH_2SiMe_2)_2N]Zr(\eta^5\text{-}C_5H_5)\}_2(\mu\text{-}\eta^1\text{:}\eta^1\text{-}N_2)$ has the bridging dinitrogen unit end-on. In this case, the MO analysis shows that the cyclopentadienyl ligand overlaps with that zirconium d orbital which could form the $\delta$-molecular orbital of the side-on mode; as a result, the end-on form is generated. A similar argument can be used to rationalize the end-on binding mode of the dinitrogen unit in the related tantalum derivatives $\{[(Pr^i_2PCH_2SiMe_2)_2N]Ta{=}CHR\}_2(\mu\text{-}\eta^1\text{:}\eta^1\text{-}N_2)$ (R = $Bu^t$, Ph), since now the alkylidene unit effectively overlaps with the same d orbital. Crystals of $\{[(Pr^i_2PCH_2SiMe_2)_2N]ZrCl\}_2(\mu\text{-}\eta^2\text{:}\eta^2\text{-}N_2)\cdot CH_3C_6H_5$ are monoclinic, $a$ = 14.103(3), $b$ = 16.233(3), and $c$ = 14.678(3) Å, $\beta$ = 114.24(1)°, $Z$ = 2, space group $P2_1/c$; those of $\{[(Pr^i_2PCH_2SiMe_2)_2N]Zr(\eta^5\text{-}C_5H_5)\}_2(\mu\text{-}\eta^1\text{:}\eta^1\text{-}N_2)\cdot 0.5$petroleum ether are also monoclinic, $a$ = 48.755(4), $b$ = 10.226(7), and $c$ = 25.987(4) Å, $\beta$ = 104.582(9)°, $Z$ = 8, space group $C2/c$. The structures were solved by heavy atom methods and were refined by full-matrix least-squares procedures to $R$ = 0.040 and 0.034 for 4158 and 7287 reflections with $I \geq 3\sigma(I)$, respectively.

## Introduction

Although dinitrogen is one of the most plentiful small molecules in the atmosphere, it is also exceedingly unreactive. Prior to 1965, the only known reactions of molecular nitrogen at ambient temperature were those with certain nitrogen-fixing bacteria and the slow formation of lithium nitride by direct reaction with lithium.[1] It was in 1965 that Allen and Senoff reported[2,3] the synthesis of the first dinitrogen complex $[Ru(NH_3)_5N_2]^{2+}$, which subsequently touched off a worldwide effort. Since that initial discovery, hundreds of dinitrogen complexes have been reported and the area has been reviewed regularly.[4-11]

It was generally believed that coordination of the otherwise stalwart dinitrogen molecule would lead to activation and, further, to its use as a feedstock for the production of ammonia under milder conditions than the Haber process and even perhaps for the formation of more complex nitrogen-containing molecules.[4] Alas, none of this has come to pass. There have been many studies, however, that do indicate that a coordinated dinitrogen is reactive to a variety of reagents to generate N–H and N–C bonds but only in stoichiometric sequences.[6,12]

Activation of the dinitrogen fragment by coordination to a metal is thought to be gauged by the change in the N–N bond length upon ligation; in free $N_2$, the bond length is 1.0975 Å.[13] Typical ranges for bond lengths of metal dinitrogen complexes are 1.10–1.16 Å for mononuclear complexes and 1.12–1.36 Å for dinuclear or higher clusters that contain the $N_2$ ligand in a bridging mode. For mononuclear metal complexes, the dinitrogen ligand normally binds in a linear, end-on mode as shown in I. As a bridging ligand in dinuclear systems,[9] the most common mode of bonding is also linear end-on, as shown in II; in this case a resonance diazenide-(2-) or hydrazide(4-) form is sometimes appropriate as well.

There are a number of other specific structural types known, as represented by III, IV, and V: the nickel–lithium cluster derivative $\{(PhLi)_6Ni_2(\mu\text{-}N_2)(Et_2O)_2\}_2$ and a related sodium derivative have been structurally characterized[14-16] as having the edge-on bridging structure type III; a complex tetranuclear titanium cluster has been shown[17] to have structure IV, and a

† E. W. R. Steacie Fellow (1990–92).
‡ NSERC of Canada Postgraduate Scholar.
§ Experimental Officer: UBC Crystallographic Service.

(1) Wilkinson, G.; Cotton, F. A. *Advanced Inorganic Chemistry*, 4th ed.; Wiley: Toronto, 1980; p 413.
(2) Allen, A. D.; Senoff, C. V. *Chem. Commun.* **1965**, 621.
(3) Senoff, C. V. *J. Chem. Ed.* **1990**, *67*, 368.
(4) Chatt, J. *J. Organomet. Chem.* **1975**, *100*, 17.
(5) Chatt, J.; Dilworth, J. R.; Richards, R. L. *Chem. Rev.* **1978**, *78*, 589.
(6) Dilworth, J. R.; Richards, R. L. In *Comprehensive Organometallic Chemistry*; G. Wilkinson, G., Stone, F. G. A., Abel, E. W., Eds.; Pergamon Press: Oxford, 1982; Vol. 8, p 1073.
(7) Henderson, R. A.; Leigh, G. J.; Pickett, C. J. *Adv. Inorg. Chem. Radiochem.* **1983**, *27*, 197.
(8) Pelikán, P.; Boca, R. *Coord. Chem. Rev.* **1984**, *55*, 55.
(9) Henderson, R. A. *Transition Met. Chem.* **1990**, *15*, 330.
(10) Richards, R. L. In *Biology and Biochemistry of Nitrogen Fixation*; Dilworth, M. J., Glenn, A. R., Es.; Elsevier: Amsterdam, 1991; p 58.
(11) Leigh, G. J. *Acc. Chem. Res.* **1992**, *25*, 177.
(12) Hidai, M.; Mizobe, Y. In *Reaction of Coordinated Ligands*; Braterman, P. S., Ed.; Plenum Press: New York, 1989; Vol. 2, p 53.
(13) Wilkinson, P. G.; Houk, N. B. *J. Chem. Phys.* **1956**, *24*, 528.
(14) Jonas, K. *Angew. Chem., Int. Ed. Engl.* **1973**, *12*, 997.
(15) Krüger, C.; Tsay, Y.-H. *Angew. Chem., Int. Ed. Engl.* **1973**, *12*, 998.
(16) Jonas, K.; Brauer, D. J.; Krüger, C.; Roberts, P. J.; Tsay, Y.-H. *J. Am. Chem. Soc.* **1976**, *98*, 74.
(17) Pez, G. P.; Apgar, P.; Crissey, R. K. *J. Am. Chem. Soc.* **1982**, *104*, 482.

0002-7863/93/1515-2782$04.00/0 

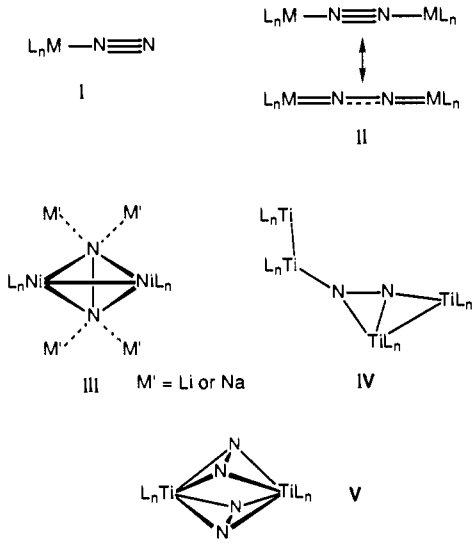


binuclear mixed-valence titanium derivative has two edge-on bridging dinitrogen units.[18]

A rare type of binding by molecular nitrogen is the side-on mode, as shown schematically in **VI** and **VII**. In mononuclear

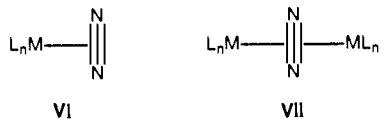


complexes, the side-on mode **VI** has been proposed[19] to be present in $Cp_2Zr(CH_2SiMe_3)N_2$ on the basis of solution ESR and IR studies, detected in matrix-isolated $Co(\eta^2\text{-}N_2)$,[20] and is a probable intermediate in end-to-end rotation of end-on derivatives of type **I**.[21] Quite recently,[22] the unusual dinuclear samarium complex $\{Cp^*_2Sm\}_2(\mu\text{-}\eta^2\text{:}\eta^2\text{-}N_2)$ was crystallographically characterized as having the symmetrically-bridging side-on mode shown in **VII**; the N–N bond length in this samarium derivative is 1.088(12) Å, which indicates no activation of the dinitrogen unit since this distance is not significantly different to that of free $N_2$. The fact that this samarium complex readily loses $N_2$ in solution indicates that the $N_2$ unit is rather weakly bound.

A recent report[23] from our laboratory outlined the preparation of a bridging side-on bound dinitrogen complex of Zr. The N–N bond length in this complex was found to be 1.548(7) Å, the longest N–N bond distance yet reported for a dinitrogen complex. In this paper we present the full details of this work and a discussion of the bonding of this complex as well as related derivatives to test the generality of certain conclusions of our bonding analysis.

## Experimental Section

**General Procedures.** All manipulations were performed under prepurified nitrogen in a Vacuum Atmospheres HE-553-2 workstation equipped with a MO-40-2H purification system or in Schlenk-type glassware. Toluene and hexanes were dried and deoxygenated by distillation from sodium–benzophenone ketyl under argon. Tetrahydrofuran was predried by refluxing over $CaH_2$ and then distilled from sodium–benzophenone ketyl under argon. Deuterated benzene ($C_6D_6$, 99.6 atom % D) and deuterated toluene ($C_7D_8$, 99.6 atom % D), purchased from MSD Isotopes, were dried over activated 4-Å molecular sieves, vacuum transferred, and taken through a freeze–pump-thaw cycle three times before use. 99% $^{15}N_2$ was obtained from Cambridge Isotopes Ltd. $TaCl_5$ (99.9%) was purchased from Aldrich Chemical Company and used as received. The complexes $ZrCl_3[N(SiMe_2CH_2PR_2)_2]$ (R = Pr$^i$, Bu$^t$, Me),[24] $Ta(CH_2\text{-}Bu^t)_2Cl_3$,[25] and $Ta(CH_2Ph)_2Cl_3$[26] were prepared according to the published procedures. NaCp·DME, where DME = 1,2-dimethoxyethane, was prepared[27] by the reaction of sodium metal with freshly cracked cyclopentadiene in dry DME under $N_2$ and crystallized directly from the reaction mixture.

The $^1H$, $^{31}P$, and $^{13}C$ NMR spectra were recorded in $C_6D_6$ or $CD_3C_6D_5$ on a Varian XL-300, a Bruker AC 200, a Bruker WH-400, or a Bruker AM-500 spectrometer. Proton spectra were referenced using the partially deuterated solvent peak as the internal reference. The $^{31}P\{^1H\}$ NMR spectra were referenced to external $P(OMe)_3$ set at +141.00 ppm relative to 85% $H_3PO_4$. The $^{13}C\{^1H\}$ NMR spectra were referenced to the $C_6D_6$ signal at 128.0 ppm. Solution $^{15}N\{^1H\}$ NMR spectra were recorded on the XL-300, referenced to external formamide set at 0.00 ppm. Solid-state $^{15}N$ NMR spectra were run on a Bruker MSL-400, referenced to solid $NH_4Cl$ set at −73.39 ppm with respect to neat formamide at 0.00 ppm. All NMR $J$ values are reported in hertz. UV–Vis spectra were recorded on a Perkin-Elmer 5523 UV–vis spectrophotometer stabilized at 20 °C. Mass spectral studies were carried out on a Kratos MS 50 using an EI source. Carbon, hydrogen, and nitrogen analyses were performed by Mr. P. Borda of this department.

**$\{[(Pr^i_2PCH_2SiMe_2)_2N]ZrCl\}_2(\mu\text{-}\eta^2\text{:}\eta^2\text{-}N_2)$ (2a).** A solution of $ZrCl_3[N(SiMe_2CH_2PPr^i_2)_2]$ (1.000 g, 1.69 mmol) in toluene (80 mL) was transferred to a thick-walled reaction flask (300 mL) equipped with a 10-mm Teflon-brand needle valve containing 0.35% Na/Hg (45 g, 6.85 mmol). The flask was then cooled to −196 °C, filled with $N_2$, sealed, and allowed to warm slowly to room temperature with stirring. The colorless solution slowly takes on the deep blue color of the product. The reaction mixture was stirred for 7 days and then filtered through a layer of Celite. The amalgam-containing residue was extracted with several 80-mL portions (approximately 800 mL) of toluene until the extracts showed no blue color. Upon removal of the toluene the product separates out as deep blue crystals (0.38 g, 38%). $^1H$ NMR ($\delta$, 500 MHz, $C_6D_6$): 2.41 (d of sept, 4 H, $P[CH(CH_3)_2]_2$, $^3J_{H\text{-}H}$ = 7.3, $^2J_{P\text{-}H}$ = 4.2); 2.15 (d of sept, 4 H, $P[CH(CH_3)_2]_2$, $^3J_{H\text{-}H}$ = 7.2, $^2J_{P\text{-}H}$ = 4.1); 1.43 (d of d, 12 H, $P[CH(CH_3)_2]_2$, $^3J_{H\text{-}H}$ = 7.3, $^3J_{P\text{-}H}$ = 14.0); 1.33 (d of d, 12 H, $P[CH(CH_3)_2]_2$, $^3J_{H\text{-}H}$ = 7.2, $^3J_{P\text{-}H}$ = 13.3); 1.29 (d of d, 12 H, $P[CH(CH_3)_2]$, $^3J_{H\text{-}H}$ = 7.3, $^3J_{P\text{-}H}$ = 12.2); 1.27 (d of d, 12 H, $P[CH(CH_3)_2]_2$, $^3J_{H\text{-}H}$ = 7.2, $^3J_{P\text{-}H}$ = 13.2); 1.07 (d of d, 4 H, $PCH_2Si$, $^2J_{H\text{-}H}$ = 13.9, $^2J_{P\text{-}H}$ = 7.0); 1.00 (d of d, 4 H, $PCH_2Si$, $^2J_{H\text{-}H}$ = 13.9, $^2J_{P\text{-}H}$ = 7.0); 0.38 (s, 12 H, $Si(CH_3)_2$); 0.33 (s, 12 H, $Si(CH_3)_2$) $^{31}P\{^1H\}$ NMR ($\delta$, 121.4 MHz, $C_6D_6$): +10.0 (s). UV–Vis: (pentane, 1-cm quartz cell): $\lambda_{max}$ = 580 nm, $\epsilon$ = 3500 L mol$^{-1}$ cm$^{-1}$. Anal. Calcd for $C_{36}H_{88}Cl_2N_4P_4Si_4Zr_2$: C, 40.54; H, 8.31; N, 5.25. Found: C, 40.65; H, 8.48; N, 5.20. MS (EI) $m/z$: 1066 $M^+$, 1023, 981, 935, 803, 350, 262.

**$\{[(Pr^i_2PCH_2SiMe_2)_2N]ZrCl\}_2(\mu\text{-}\eta^2\text{:}\eta^2\text{-}^{15}N_2)$.** The $^{15}N_2$ analogue was prepared similarly by introducing $^{15}N_2$ gas into the flask containing the degassed reaction mixture. Workup was carried out under unlabeled $N_2$. $^{15}N\{^1H\}$ NMR ($\delta$, 30.406 MHz, $C_7D_8$): 350.92 (s). $^{15}N$ MAS NMR ($\delta$, 40.60 MHz): 345 (s). MS (EI) $m/z$: 1068 $M^+$, 1025, 983, 937, 805, 350, 262.

**$\{[(Bu^t_2PCH_2SiMe_2)_2N]ZrCl\}_2(\mu\text{-}\eta^2\text{:}\eta^2\text{-}N_2)$ (2b).** The same procedure as was used for the above compound resulted in only a trace yield of product. The best results came from stirring 2 equiv of sodium sand (12 mg, 0.52 mmol) with $ZrCl_3[N(SiMe_2CH_2PBu^t_2)_2]$ (0.161 mg, 0.249 mmol) under 1 atm of $N_2$ in toluene (60 mL) for 2 weeks. The yield of product (66 mg, 0.053 mmol) was 42%. $^1H$ NMR ($\delta$, 300 MHz, $C_7D_8$): at 60 °C, 1.52 (br s, 36 H, $P[C(CH_3)_3]_2$); 1.29 (br m, 36 H, $P[C(CH_3)_3]_2$); 1.09 (d of d, 8 H, $J$ = 12, 2, $PCH_2Si$); 0.43 (s, 12 H, $Si(CH_3)_2$); 0.28 (s, 12 H, $Si(CH_3)_2$); at 20 °C, 1.59 (t, 18 H, $P[C(CH_3)_3]_2$, $^3J_{P\text{-}H}$ = 6.3); 1.47 (t, 18 H, $P[C(CH_3)_3]_2$, $^3J_{P\text{-}H}$ = 6.0); 1.29 (m, 36 H, $P[C(CH_3)_3]_2$); 1.1–0.8 (m, 8 H, $PCH_2Si$); 0.47 (s, 6 H, $Si(CH_3)_2$); 0.44 (s, 6 H, $Si(CH_3)_2$); 0.32 (s, 6 H, $Si(CH_3)_2$); 0.29 (s, 6 H, $Si(CH_3)_2$). $^{31}P\{^1H\}$ NMR ($\delta$, 121.4 MHz $C_7D_8$): at 20 °C, +35.7; at −30° C, AB quartet at 35.1 (d, $^2J_{P\text{-}P}$ = 75.2); 34.8 (d, $^2J_{P\text{-}P}$ = 75.2). Anal. Calcd for $C_{44}H_{104}Cl_2N_4P_4Si_4Zr_2$: C, 44.83; H, 8.89; N, 4.75; Cl, 6.01. Found: C, 45.10; H, 9.10; N, 4.87; Cl, 5.90.

(18) Duchateau, R.; Gambarotta, S.; Beydoun, N.; Bensimon, C. *J. Am. Chem. Soc.* **1991**, *113*, 8986.
(19) Jeffery, J.; Lappert, M. F.; Riley, P. I. *J. Organomet. Chem.* **1979**, *181*, 25.
(20) Ozin, G. A.; Vander Voet, A. *Can. J. Chem.* **1973**, *51*, 637.
(21) Cusanelli, A.; Sutton, D. *J. Chem. Soc., Chem. Commun.* **1989**, 1719.
(22) Evans, W. J.; Ulibarri, T. A.; Ziller, J. W. *J. Am. Chem. Soc.* **1988**, *110*, 6877.
(23) Fryzuk, M. D.; Haddad, T. S.; Rettig, S. J. *J. Am. Chem. Soc.* **1990**, *112*, 8185.
(24) Fryzuk, M. D.; Carter, A.; Westerhaus, A. *Inorg. Chem.* **1985**, *24*, 642.
(25) Schrock, R. R.; Fellmann, J. D. *J. Am. Chem. Soc.* **1978**, *100*, 3359.
(26) Messerle, L. W.; Jennische, P.; Schrock, R. R.; Stucky, G. *J. Am. Chem. Soc.* **1980**, *102*, 6744.
(27) Smart, J. C.; Curtis, C. J. *Inorg. Chem.* **1977**, *16*, 1788.

**$Zr(\eta^5\text{-}C_5H_5)Cl_2[N(SiMe_2CH_2PPr^i_2)_2]$ (3a).** To a solution of $ZrCl_3[N(SiMe_2CH_2PPr^i_2)_2]$ (4.040 g, 6.84 mmol) in toluene (150 mL) was added solid NaCp·DME (1.340 g, 7.52 mmol) at room temperature. The reaction mixture was stirred for 16 h, and then the salt (NaCl) was removed by filtering through Celite. The filtrate was concentrated to 15 mL, and hexanes were added until the solution turned turbid; cooling at −30 °C gave yellow hexagonal crystals (3.16 g, 75%). $^1$H NMR (δ, 300 MHz, $C_6D_6$): 0.64 (s, 12 H, $Si(CH_3)_2$); 1.00 (m, 28 H, $P[CH(CH_3)_2]_2$, $SiCH_2P$); 2.12 (m, 4 H, $P[CH(CH_3)_2]_2$); 6.15 (t, ~5 H, $C_5H_5$, $^3J_{H\text{-}P}$ = 1.4). $^{31}P\{^1H\}$ NMR (δ, 121.421 MHz, $C_6D_6$): 16.11 (s). $^{13}C\{^1H\}$ NMR (δ, 50.323 MHz, $C_6D_6$): 7.82 (s, $Si(CH_3)_2$); 8.71 (s, $SiCH_2P$); 18.74 (s, $P[CH(CH_3)_2]_2$); 18.96 (s, $P[CH(CH_3)_2]_2$); 24.72 (t, $P[CH(CH_3)_2]_2$, $^2J_{C\text{-}P}$ = 4.5); 116.00 (s, $C_5H_5$). Anal. Calcd for $C_{23}H_{49}Cl_2NP_2Si_2Zr$: C, 44.56; H, 7.97; N, 2.26. Found: C, 44.72; H, 8.20; N, 2.32.

**$\{[(Pr^i_2PCH_2SiMe_2)_2N]Zr(\eta^5\text{-}C_5H_5)\}_2(\mu\text{-}\eta^1\text{:}\eta^1\text{-}N_2)$ (4a).** A solution of $Zr(\eta^5\text{-}C_5H_5)Cl_2[N(SiMe_2CH_2PPr^i_2)_2]$ (0.980 g, 1.58 mmol) in toluene (60 mL) was transferred to a thick-walled reaction flask (300 mL) containing Na/Hg (85 g of 0.33% amalgam, 12.17 mmol of Na). The reaction flask was sealed under $N_2$ as described in the synthesis of $\{[(Pr^i_2PCH_2SiMe_2)_2N]ZrCl\}_2(\mu\text{-}\eta^2\text{:}\eta^2\text{-}N_2)$. Upon warming to room temperature the reaction mixture quickly turned green (1 h) and then slowly turned deep brown. After the disappearance of the green color (3 days) the solution was filtered through a layer of Celite. The amalgam was extracted with 15-mL portions of toluene (total of 60 mL) until the extracts showed no brown color. Removal of the solvent gave a dark brown powder (0.860 g, 96%) in high purity (>95% by NMR spectroscopy). The product was crystallized from a 1:1 mixture of toluene and pentane. $^1$H NMR (δ, 300 MHz, $C_6D_6$): 0.28 (s, 12 H, $Si(CH_3)_2$); 0.33 (s, 12 H, $Si(CH_3)_2$); 1.18 (m, 48 H, $P[CH(CH_3)_2]_2$); 1.54 (br, 8 H, $SiCH_2P$); 1.88 (m, 4 H, $P[CH(CH_3)_2]_2$); 2.54 (m, 4 H, $P[CH(CH_3)_2]_2$); 6.11 (br, ~10 H, $C_5H_5$). $^{31}P\{^1H\}$ NMR (δ, 121.421 MHz, $C_7D_8$): at 20 °C, 20.26 (s); at −40 °C, AB quartet at 19.95 (d, $^2J_{P\text{-}P}$ = 80.7) and 20.57 (d, $^2J_{P\text{-}P}$ = 80.7). $^{13}C\{^1H\}$ NMR (δ, 50.323 MHz, $C_6D_6$): 6.46 (s, $Si(CH_3)_2$); 6.71 (s, $Si(CH_3)_2$); 11.63 (s, $SiCH_2P$); 18.40 (s, $P[CH(CH_3)_2]_2$); 20.94 (s, $P[CH(CH_3)_2]_2$); 21.35 (s, $P[CH(CH_3)_2]_2$); 101,37 (s, $C_5H_5$). Anal. Calcd for $C_{46}H_{98}N_4P_4Si_4Zr_2 \cdot 0.5C_5H_{12}$: C, 50.13; H, 9.02; N, 4.82. Found: C, 50.11; H, 8.94; N, 4.90. MS (EI) *m/z*: 1124 $M^+$, 1081, 993, 949, 732, 688, 562, 519, 497, 475, 445, 431, 350, 262.

**$\{[(Pr^i_2PCH_2SiMe_2)_2N]Zr(\eta^5\text{-}C_5H_5)\}_2(\mu\text{-}\eta^1\text{:}\eta^1\text{-}{}^{15}N_2)$.** The $^{15}N$ analogue was prepared similarly by introducing $^{15}N_2$ gas into the flask containing the degassed reaction mixture. Workup was carried out under unlabeled $N_2$. $^{15}N\{^1H\}$ NMR (δ, 30.406 MHz, $C_7D_8$): 353.95 (s). MS (EI) *m/z*: 1126 $M^+$, 1083, 995, 951, 734, 690, 563, 520, 498, 476, 446, 432, 350, 262.

**Reaction of $\{[(Pr^i_2PCH_2SiMe_2)_2N]ZrCl\}_2(\mu\text{-}\eta^2\text{:}\eta^2\text{-}{}^{15}N_2)$ with NaCp·DME.** To a solution of $\{[(Pr^i_2PCH_2SiMe_2)_2N]ZrCl\}_2(\mu\text{-}\eta^2\text{:}\eta^2\text{-}{}^{15}N_2)$ (30 mg, 0.028 mmol) in THF (4 mL) was added a solution of NaCp·DME (11 mg, 0.062 mmol) dissolved in THF (2 mL) under an atmosphere of unlabeled $N_2$. A control experiment was set up under an atmosphere of argon. Both reactions were stirred at room temperature until they turned brown (6 days). The solvent was removed in vacuo, and extraction of the crude product with pentane (5 mL) gave a brown powder after the pentane was removed. The brown powder was shown to be $\{[(Pr^i_2PCH_2SiMe_2)N]Zr(\eta^5\text{-}C_5H_5)\}_2(\mu\text{-}N_2)$ by NMR. A similar reaction carried out in an NMR tube showed clean conversion of the side-on complex to the end-on complex. MS (EI) *m/z*: 1126 $M^+$, 1083, 995, 951, 734, 690.

**$Ta(=CHBu^t)Cl_2[N(SiMe_2CH_2PPr^i_2)_2]$ (5).** To a stirred yellow $Et_2O$ solution (200 mL) of $Ta(CH_2Bu^t)_2Cl_3$ (1.841 g, 4.291 mmol) at room temperature was added an $Et_2O$ solution (30 mL) of $LiN(SiMe_2CH_2PPr^i_2)_2$ (1.713 g, 4.292 mmol) over 5 min. Within 30 min the solution turned purple. After the solution was stirred for 24 h the ether was removed under vacuum, and the crude product was extracted with hexanes (100 mL) and filtered through a layer of Celite to remove LiCl. Concentration of the solution to 25 mL followed by cooling to −40 °C overnight yielded 2.002 g of purple crystalline **1**. Further concentration of the solution to 5 mL gave another 513 mg (total yield 82%). $^1$H NMR ($C_6D_6$, δ): 7.19 (t, $CHBu^t$, 1 H, $^3J_{H\ P}$ = 1.5); 2.79 (t of sept, $PCH(CH_3)_2$, 2 H, $[^2J_{H\ P} + {}^4J_{H\ P}]/2$ = 3, $^3J_{H\ H}$ = 7); 2.33 (t, of sept, $PCH(CH_3)_2$, 2 H, $[^2J_{H\ P} + {}^4J_{H\ P}]/2$ = 3, $^3J_{H\ H}$ = 7); 1.59 (d of t, $PCH_2$, 2 H, $^2J_{H\ H}$ = 14, $[^2J_{H\ P} + {}^4J_{H\ P}]/2$ = 3); 1.44 (s, $CH(CH_3)_3$, 9 H); 1.43 (d of d, $PCH(CH_3)_2$, 6 H, $^3J_{H\ P}$ = 14, $^3J_{H\ H}$ = 7); 1.21 (d of d, $PCH(CH_3)_2$, 6 H, $^3J_{H\ P}$ = 15, $^3J_{H\ H}$ = 7); 1.18 (d of d, $PCH(CH_3)_2$, 6 H, $^3J_{H\ P}$ = 14, $^3J_{H\ H}$ = 7); 1.13 (d of d, $PCH(CH_3)_2$, 6 H, $^3J_{H\ P}$ = 14, $^3J_{H\ H}$ = 7); 1.04 (d of t, $PCH_2$, 2 H, $^2J_{H\ H}$ = 14, $[^2J_{H\ P} + {}^4J_{H\ P}]/2$ = 3); 0.43 (s, $SiCH_3$, 6 H); 0.24 (s, $SiCH_3$, 6 H). $^{31}P\{^1H\}$ NMR ($C_6D_6$, δ): 37.7 (s). $^{13}C\{^1H\}$ NMR ($C_6D_6$, δ): 263.3 (d, $CHBu^t$, $^1J_{C\ H}$ = 89); 45.5 (s, $C(CH_3)_3$); 36.1 (s, $C(CH_3)_2$); 28.3 (s, $PCH(CH_3)_2$); 26.8 (s, $PCH(CH_3)_2$); 20.9 (s, $PCH(CH_3)_2$); 20.1 (s, $PCH(CH_3)_2$); 19.4 (s, $PCH(CH_3)_2$); 18.8 (s, $PCH(CH_3)_2$); 14.7 (s, $PCH_2$); 5.3 (s, $SiCH_3$); 3.3 (s, $SiCH_3$). MW calcd 715, found 701 g mol$^{-1}$. Anal. Calcd for $C_{23}H_{54}Cl_2NP_2Si_2Ta$: C, 38.66; H, 7.62; N, 1.96. Found: C, 38.37; H, 7.82; N, 1.79.

**$Ta(=CHPh)Cl_2[N(SiMe_2CH_2PPr^i_2)_2]$ (6).** To a stirred orange-red $Et_2O$ solution (200 mL) of $Ta(CH_2Ph)_2Cl_3$ (4.591 g, 9.782 mmol) at room temperature was added an $Et_2O$ solution (30 mL) of $LiN(SiMe_2CH_2PPr^i_2)_2$ (3.911 g, 9.781 mmol) over 5 min. The metathesis reaction was evident by the formation of LiCl, but no color change occurred for 6 h. After the solution was stirred for 72 h the ether was removed under vacuum, and the crude product was extracted with toluene (200 mL) and filtered through a layer of Celite to remove LiCl. Concentration of the solution to 50 mL followed by cooling to −40 °C overnight yielded 6.573 g of deep green crystalline **4** (91%). $^1$H NMR ($C_6D_6$, δ): 9.08 (t, $CHPh$, 1 H, $^3J_{H\text{-}P}$ = 1.6); 7.56 (d, $H_o$, 2 H, $^3J_{H\text{-}H}$ = 7); 7.35 (t, $H_m$, 2 H, $^3J_{H\text{-}H}$ = 7); 6.69 (t, $H_p$, 1 H, $^3J_{H\text{-}H}$ = 7); 2.67 (t of sept, $PCH(CH_3)_2$, 2 H, $^3J_{H\text{-}H}$ = 7, $[^2J_{H\text{-}P} + {}^4J_{H\text{-}P}]/2$ = 4); 2.09 (t of sept, $PCH(CH_3)_2$, 2 H, $^3J_{H\text{-}H}$ = 7, $[^2J_{H\text{-}P} + {}^4J_{H\text{-}P}]/2$ = 4); 1.38 (d of d, $PCH(CH_3)_2$, 6 H, $^3J_{H\text{-}P}$ = 16, $^3J_{H\text{-}H}$ = 7); 1.18 (d of d, $PCH(CH_3)_2$, 6 H, $^3J_{H\text{-}P}$ = 15, $^3J_{H\text{-}H}$ = 7); 1.09 (m, $PCH_2$, 4 H); 1.02 (d of d, $PCH(CH_3)_2$, 6 H, $^3J_{H\text{-}P}$ = 14, $^3J_{H\text{-}H}$ = 7); 0.98 (d of d, $PCH(CH_3)_2$, 6 H, $^3J_{H\text{-}P}$ = 16, $^3J_{H\text{-}H}$ = 7); 0.41 (s, $SiCH_3$, 6 H); 0.29 (s, $SiCH_3$, 6 H). $^{31}P\{^1H\}$ NMR ($C_6D_6$, δ): 40.1 (s). $^{13}C\{^1H\}$ NMR ($C_6D_6$, δ): 255.3 (d, $CHPh$, $^1J_{C\text{-}H}$ = 98); 145.2 (s, $C_{ipso}$ of phenyl); 133.2 (s, $C_o$ of phenyl); 131.1 (s, $C_m$ of phenyl); 125.4 (s, $C_p$ of phenyl); 27.4 (s, $PCH(CH_3)_2$); 25.6 (s, $PCH(CH_3)_2$); 19.8 (s, $PCH(CH_3)_2$); 19.4 (s, $PCH(CH_3)_2$); 19.1 (s, $PCH(CH_3)_2$); 18.1 (s, $PCH(CH_3)_2$); 13.1 (s, $PCH_2$); 4.8 (s, $SiCH_3$); 3.7 (s, $SiCH_3$). Anal. Calcd for $C_{25}H_{50}Cl_2NP_2Si_2Ta$: C, 40.87; H, 6.86; N, 1.91. Found: C, 40.97; H, 7.05; N, 2.08.

**$\{[(Pr^i_2PCH_2SiMe_2)_2N]Ta(=CHBu^t)Cl\}_2(\mu\text{-}N_2)$ (7).** In the glovebox, a ~1% sodium amalgam was generated in a 350-mL reactor bomb by dissolving 27 mg of Na (1.2 mmol) in 2.7 g of Hg. A 25-mL toluene solution containing 211 mg (0.295 mmol) of $Ta(=CHBu^t)Cl_2[N(SiMe_2CH_2PPr^i_2)_2]$ (**5**) was then added to the amalgam. The reactor bomb was sealed and taken to a vacuum line. The reactor bomb was degassed three times and cooled to −196 °C. Dinitrogen was introduced at −196 °C, and the reactor bomb was sealed. The solution was slowly warmed to room temperature and stirred vigorously. The purple solution gradually turned yellow in color as NaCl formed. After 48 h the solution was filtered through a medium porosity frit with the aid of Celite, being careful to leave the mercury residues behind. Concentration to 5 mL and cooling to −40 °C yielded 171 mg of **8** (88%). $^1$H NMR ($C_6D_6$, δ): 7.20 (br s, $CHBu^t$, 2 H); 2.41 (br t of pentets, $PCH(CH_3)_2$, 4 H); 2.09 (t of pentets, $PCH(CH_3)_2$, 4 H, $^3J_{H\text{-}H}$ = 7, $[^2J_{H\text{-}P} + {}^4J_{H\text{-}P}]/2$ = 3); 1.44 (d of d, $PCH(CH_3)_2$, 12 H, $^3J_{H\text{-}H}$ = 7, $^3J_{H\text{-}P}$ = 14); 1.42 (s, $CH(CH_3)_2$, 18 H); 1.34 (d of d, $PCH(CH_3)_2$, 12 H, $^3J_{H\text{-}H}$ = 7, $^3J_{H\text{-}P}$ = 15); 1.32 (d of d, $PCH(CH_3)_2$, 12 H, $^3J_{H\text{-}H}$ = 7, $^3J_{H\text{-}P}$ = 14); 1.26 (d of d, $PCH(CH_3)_2$, 12 H, $^3J_{H\text{-}H}$ = 7, $^3J_{H\text{-}P}$ = 14); 1.06 (d of t, $PCH_2$, 4 H, $^2J_{H\text{-}H}$ = 15, $[^2J_{H\text{-}P} + {}^4J_{H\text{-}P}]/2$ = 3); 1.02 (d of t, $PCH_2$, 4 H, $^2J_{H\text{-}H}$ = 15, $[^2J_{H\text{-}P} + {}^4J_{H\text{-}P}]/2$ = 3); 0.44 (s, $SiCH_3$, 12 H); 0.36 (s, $SiCH_3$, 12 H). $^{31}P\{^1H\}$ NMR ($C_6D_6$, δ): 48.8 (br s). $^{15}N\{^1H\}$ NMR ($C_7D_8$, δ): 419 (s). MW calcd 1316, found 1227 g mol$^{-1}$. Anal. Calcd for $C_{46}H_{108}N_4P_4Si_4Ta_2$: C, 41.99; H, 8.27; N, 4.26. Found: C, 41.43; H, 8.43; N, 4.09.

**$\{[(Pr^i_2PCH_2SiMe_2)_2N]Ta(=CHPh)Cl\}_2(\mu\text{-}N_2)$.** The preparation of **8** is identical to the procedure outlined for complex **7** above. $Ta(=CHPh)Cl_2[N(SiMe_2CH_2PPr^i_2)_2]$ (**6**) (1.000 g, 1.361 mmol) yielded 736 mg of **8** (79%). $^1$H NMR ($C_6D_6$, δ): 9.35 (br s, $CHPh$, 2 H); 7.47 (d, $H_o$ of phenyl, 4 H, $^3J_{H\text{-}H}$ = 7); 7.35 (t, $H_m$ of phenyl, 4 H, $^3J_{H\text{-}H}$ = 7); 6.84 (t, $H_p$ of phenyl, 2 H, $^3J_{H\text{-}H}$ = 7); 2.40 (br sept, $PCH(CH_3)_2$, 4 H, $^3J_{H\text{-}H}$ = 7); 2.08 (br sept, $PCH(CH_3)_2$, 4 H); 1.28 (overlapping d of d, $PCH(CH_3)_2$, 24 H, $^3J_{H\text{-}P}$ = 14, $^3J_{H\text{-}H}$ = 7); 1.19 (overlapping d of d, $PCH(CH_3)_2$, 24 H, $^3J_{H\text{-}P}$ = 13, $^3J_{H\text{-}H}$ = 7); 0.81 (overlapping d of t, $PCH_2$, 8 H, $^2J_{H\text{-}H}$ = 15, $[^2J_{H\text{-}P} + {}^4J_{H\text{-}P}]/2$ = 3); 0.51 (s, $SiCH_3$, 12 H); 0.39 (s, $SiCH_3$, 12 H). $^{31}P\{^1H\}$ NMR ($C_6D_6$, δ): 51.1 (s). Anal. Calcd for $C_{50}H_{100}N_4P_4Si_4Ta_2$: C, 44.30; H, 7.44; N, 4.13. Found: C, 44.72; H, 7.52; N, 3.90.

**Hydrazine Analysis.** The two zirconium dinitrogen complexes $\{[(Pr^i_2PCH_2SiMe_2)_2N]ZrCl\}_2(\mu\text{-}\eta^2\text{:}\eta^2\text{-}N_2)$ (**2a**) and $\{[(Pr^i_2PCH_2SiMe_2)_2N]Zr(\eta^5\text{-}C_5H_5)\}_2(\mu\text{-}\eta^1\text{:}\eta^1\text{-}N_2)$ (**4a**) were decomposed by addition of excess dry HCl gas to toluene solutions of the corresponding complexes; extraction of the organic phase with distilled $H_2O$ and analysis colorimetrically by the method of Watt and Chrisp[28] gave the following results: (i) $\{[(Pr^i_2PCH_2SiMe_2)_2N]ZrCl\}_2(\mu\text{-}\eta^2\text{:}\eta^2\text{-}N_2)$ gave 0.97 ± 0.05 equiv $N_2H_4$ for

(28) Watt, G. W.; Chrisp, J. D. *Anal. Chem.* **1952**, *24*, 2006.

four separate determinations and (ii) $\{[(Pr^i_2PCH_2SiMe_2)_2N]Zr(\eta^5\text{-}C_5H_5)\}_2(\mu\text{-}\eta^1\text{:}\eta^1\text{-}N_2)$ gave 1.05 ± 0.05 equiv $N_2H_4$ for four separate determinations.

**Molecular Orbital Calculations.** All molecular orbital calculations were performed on the CAChe Worksystem, a product developed by Tektronix. The parameters used in the INDO/1 semiempirical molecular orbital calculations on the model compound $[(H_3P)_2(NH_2)ZrCl]_2(\mu\text{-}\eta^2\text{:}\eta^2\text{-}N_2)$ were taken from the literature.[29] A full list of eigenvalues and symmetry labels can be found in the supplementary material. The bond lengths were taken from the X-ray crystal structure analysis[23] of $\{[(Pr^i_2\text{-}PCH_2SiMe_2)_2N]ZrCl\}_2(\mu\text{-}\eta^2\text{:}\eta^2\text{-}N_2)$, and the model was restricted to $C_{2h}$ symmetry. The Cartesian coordinates of the models can be found in the supplementary material. For all models the following standard bond lengths were used: P–H, 1.380 Å; C–H, 1.090 Å; N–H, 1.070 Å.

The parameters used for the Extended Hückel calculation of the model fragment $\{H_3P\}_2Ta(=CH_2)(NH_2)$ were taken from the literature[30] and are listed in the supplementary material. The bond lengths and angles used for the tantalum model are as follows: Ta–N, 2.175 Å; Ta–P, 2.770 Å; Ta–C, 1.930 Å; P–Ta–P, 140.0°; C–Ta–N, 140.0°. The Cartesian coordinates of the models can be found in the supplementary material.

The parameters used for the Extended Hückel calculations of the zirconium model fragments *trans*-$Zr(NH_2)Cl(PH_3)_2$ and *trans*-$Zr(\eta^5\text{-}C_5H_5)NH_2(PH_3)_2$ were taken from the literature[31] and are listed in the supplementary material. The bond lengths and angles used for the model are as follows: Zr–N, 2.175 Å; Zr–P, 2.770 Å; Zr–Cl, 2.493 Å; P–Zr–P, 140.0°; Cl–Zr–N, 140.0°. The Cartesian coordinates of the models can be found in the supplementary material.

**X-ray Crystallographic Analyses.** Crystallographic data for $\{[(Pr^i_2\text{-}PCH_2SiMe_2)_2N]ZrCl\}_2(\mu\text{-}\eta^2\text{:}\eta^2\text{-}N_2)\cdot CH_3C_6H_5$ (**2a**·$CH_3C_6H_5$) and $\{[(Pr^i_2\text{-}PCH_2SiMe_2)_2N]Zr(\eta^5\text{-}C_5H_5)\}_2(\mu\text{-}\eta^1\text{:}\eta^1\text{-}N_2)\cdot 0.5C_6H_{14}$ (**4a**·$0.5C_6H_{14}$)[32] appear in Table I. The final unit cell parameters were obtained by least-squares fitting of the setting angles for 25 reflections with $2\theta$ = 65.0–87.3° for **2a** and 31.8–35.5° for **4a**. The intensities of three standard reflections, measured every 250 reflections throughout the data collections, remained constant for both data collections. The data were processed[33] and corrected for Lorentz and polarization effects and for absorption (empirical, based on azimuthal scans for three reflections).

Both structures were solved by heavy atom methods; the coordinates of the Zr, Si, and P atoms were determined from the Patterson functions and those of the remaining non-hydrogen atoms from subsequent difference Fourier syntheses. Complex **2a** has exact crystallographic inversion symmetry. The structure analysis of **4a** was initiated in the centrosymmetric space group $C2/c$ on the basis of the $E$-statistics and the Patterson function, and this choice was confirmed by subsequent successful solution and refinement of the structure. One isopropyl group of **2a** was found to be orientationally disordered, and the thermal parameters of one $SiMe_2$ moiety indicated conformational disordering of one of the two crystallographically distinct ZrPCSiN chelate rings. Site occupancy factors for both 2-fold disordered portions of the structure were determined by refinement with fixed (and equal) isotropic thermal parameters. In the final stages of refinement the occupancy factors were kept fixed and the thermal parameters refined for all of the disordered atoms. Atoms on the periphery of the **2a** molecule all display a high degree of thermal motion at 21 °C, but the central portion of the structure (the Zr atoms and all atoms bonded to the metals) is well-defined and shows no evidence of disorder. In the structure of **4a** there were two 2-fold disordered isopropyl groups; these were treated in the same way as described above for **2a**.

Both structures contain messy regions of disordered solvent: a toluene molecule disordered about a center of symmetry in **2a** and a petroleum ether moiety disordered about a 2-fold axis in **4a**. For **2a**, several models incorporating 2–4 partially occupied rigid groups were tested and eventually discarded in favor of the aesthetically less pleasing model based on refining the four largest peaks as carbon. The latter model resulted in anomalous metrical parameters but accounted better for the electron density in the region. The four prominent peaks in the solvent region of **4a** were included in the model; the largest three (one of these on the 2-fold axis) were refined with full occupancy and the fourth assigned an occupancy of 0.5 on the basis of the Fourier map peak height. This model accounted for the majority of electron density in the solvent region of **4a**, the largest residual peak in this region being <0.3 eÅ$^{-3}$.

All non-hydrogen atoms of both complexes (with the exception of C(22) in **2a** and the four solvent carbon atoms C(47–50) in **4a**) were refined with anisotropic thermal parameters. Hydrogen atoms were fixed in idealized positions (C–H = 0.98 Å, $B_H = 1.2\ B_{\text{bonded atom}}$). Hydrogen atoms associated with the solvent in **4a** were not included in the calculations. A correction for secondary extinction was applied for **2a**, the final value of the extinction coefficient being $1.04(7) \times 10^{-6}$. Neutral atom scattering factors for all atoms and anomalous dispersion corrections for the non-hydrogen atoms were taken from the literature.[34] Selected bond lengths and selected bond angles appear in Tables II and III, respectively. Final atomic coordinates and equivalent isotropic thermal parameters, hydrogen atom parameters, anisotropic thermal parameters, complete tables of bond lengths and bond angles, torsion angles, intermolecular contacts, and least-squares planes are included as supplementary material.

**Table I.** Crystallographic Data[a]

| | **2a**·$CH_3C_6H_5$ | **4a**·$0.5C_6H_{14}$[32] |
|---|---|---|
| formula | $C_{36}H_{88}Cl_2N_4P_4Si_4Zr_2\cdot C_7H_8$ | $C_{46}H_{96}N_4P_4Si_4Zr_2\cdot 0.5C_6H_{14}$ |
| fw | 1158.84 | 1167.06 |
| color, habit | dark blue-black, plate | brown, prism |
| crystal size, mm$^3$ | 0.05 × 0.20 × 0.20 | 0.12 × 0.25 × 0.45 |
| crystal system | monoclinic | monoclinic |
| space group | $P2_1/c$ | $C2/c$ |
| $a$, Å | 14.103(3) | 48.755(4) |
| $b$, Å | 16.233(3) | 10.226(7) |
| $c$, Å | 14.678(3) | 25.987(4) |
| $\beta$, deg | 114.24(1) | 104.582(9) |
| $V$, Å$^3$ | 3064(1) | 12 539(9) |
| $Z$ | 2 | 8 |
| $\rho_{calc}$, g/cm$^3$ | 1.256 | 1.236 |
| $F(000)$ | 1224 | 4968 |
| radiation (λ, Å) | Cu (1.541 78) | Mo (0.710 69) |
| $\mu$, cm$^{-1}$ | 56.60 | 5.34 |
| trans factors (relative) | 0.43–1.00 | 0.97–1.00 |
| scan type | $\omega$–$2\theta$ | $\omega$ |
| scan range, deg in $\omega$ | 1.00 + 0.20 tan $\theta$ | 0.91 + 0.35 tan $\theta$ |
| scan rate, deg/min | 16 | 32 |
| data collected | $+h,+k,\pm l$ | $+h,+k,\pm l$ |
| $2\theta_{max}$, deg | 155 | 55 |
| crystal decay, % | negligible | negligible |
| total no. of reflcns | 7046 | 15 389 |
| no. of unique reflcns | 6783 | 15 197 |
| $R_{merge}$ | 0.035 | 0.025 |
| reflcns with $I \geq 3\sigma(I)$ | 4158 | 7287 |
| no. of variables | 303 | 573 |
| $R$ | 0.040 | 0.034 |
| $R_w$ | 0.049 | 0.035 |
| gof | 1.71 | 1.40 |
| max $\Delta/\sigma$ (final cycle) | 0.01 | 0.21 |
| residual density e/Å$^3$ | −0.50 to 0.47 | −0.27 to 0.37 |

[a] $T$ = 294 K, Rigaku AFC6S diffractometer, graphite monochromator, takeoff angle 6.0°, aperture 6.0 × 6.0 mm$^2$ at a distance of 285 mm from the crystal, stationary background counts at each end of the scan (scan/background time ratio 2:1, up to 8 rescans), $\sigma^2(F^2) = [S^2(C + 4B) + (pF^2)^2]/Lp^2$ ($S$ = scan rate, $C$ = scan count, $B$ = normalized background count, $p$ = 0.03 for **2a** and 0.02 for **4a**), function minimized $\sum w(|F_o| - |F_c|)^2$ where $w = 4F_o^2/\sigma^2(F_o^2)$, $R = \sum||F_o| - |F_c||/\sum|F_o|$, $R_w = (\sum w(|F_o| - |F_c|)^2/\sum w|F_o|^2)^{1/2}$, and gof = $[\sum w(|F_o| - |F_c|)^2/(m - n)]^{1/2}$. Values given for $R$, $R_w$, and gof are based on those reflections with $I \geq 3\sigma(I)$.

## Results and Discussion

The reduction of $ZrCl_3[N(SiMe_2CH_2PPr^i_2)_2]$ (**1a**) with 2 equiv or more of sodium–mercury amalgam (Na/Hg) in toluene under an atmosphere of $N_2$ for 5–7 days results in the formation of a deep blue solution which, after filtration and concentration, deposits dark blue-black crystals having the formula $\{[(Pr^i_2PCH_2\text{-}$

(29) Anderson, W. P.; Cundari, T. R.; Drago, R. S.; Zerner, M. C. *Inorg. Chem.* **1990**, *29*, 1.
(30) Hoffman, D. M.; Hoffmann, R.; Fisel, C. R. *J. Am. Chem. Soc.* **1982**, *104*, 3858.
(31) Hoffmann, R. *J. Chem. Phys.* **1963**, *39*, 1397.
(32) The asymmetric unit in the structure of **4a** contains $^1/_2$ molecule of "petroleum ether" solvate that has been assumed to have the formula $C_6H_{14}$ for the calculation of relevant crystallographic parameters.
(33) TEXSAN/TEXRAY structure analysis package, Version 5.1; Molecular Structure Corporation, 1985.
(34) *International Tables for X-Ray Crystallography*; Kynoch Press: Birmingham, U.K., 1974; Vol. IV, pp 99–102 and 149. (Present distributor Kluwer Academic Publishers: Dordrecht, The Netherlands.)

**Table II.** Selected Bond Lengths (Å) from X-ray Analyses of **2a**·$CH_3C_6H_5$ and **4a**·0.5$C_6H_{14}$[32]

{[$(R_2PCH_2SiMe_2)_2N$]ZrCl}$_2(\mu$-$\eta^2$:$\eta^2$-$N_2$) **2a**

| atom | atom | distance | atom | atom | distance |
|---|---|---|---|---|---|
| Zr(1) | Cl(1) | 2.493(1) | Zr(1) | N(2)′ | 2.027(4) |
| Zr(1) | P(1) | 2.764(1) | Si(1) | N(1) | 1.713(4) |
| Zr(1) | P(2) | 2.772(1) | Si(2) | N(1) | 1.746(8) |
| Zr(1) | N(1) | 2.175(3) | Si(2A) | N(1) | 1.71(1) |
| Zr(1) | N(2) | 2.024(4) | N(2) | N(2)′ | 1.548(7) |

{[$(Pr^i_2PCH_2SiMe_2)_2N$]Zr($\eta^5$-$C_5H_5$)}$_2(\mu$-$\eta^1$:$\eta^1$-$N_2$) **4a**

| atom | atom | distance | atom | atom | distance |
|---|---|---|---|---|---|
| Zr(1) | Cp(1) | 2.294(2) | Zr(2) | Cp(2) | 2.286(2) |
| Zr(1) | P(1) | 2.816(1) | Zr(2) | P(3) | 2.778(1) |
| Zr(1) | P(2) | 2.776(1) | Zr(2) | P(4) | 2.828(1) |
| Zr(1) | N(1) | 2.306(3) | Zr(2) | N(2) | 2.303(3) |
| Zr(1) | N(3) | 1.920(3) | Zr(2) | N(4) | 1.923(3) |
| N(3) | N(4) | 1.301(3) | | | |

**Table III.** Selected Bond Angles (deg) from X-ray Analyses of **2a**·$CH_3C_6H_5$ and **4a**·0.5$C_6H_{14}$[32]

{[$(Pr^i_2PCH_2SiMe_2)_2N$]ZrCl}$_2(\mu$-$\eta^2$:$\eta^2$-$N_2$) **2a**

| atom | atom | atom | angle | atom | atom | atom | angle |
|---|---|---|---|---|---|---|---|
| Cl(1) | Zr(1) | P(1) | 86.39(5) | Zr(1) | N(2)′ | N(2) | 67.5(2) |
| Cl(1) | Zr(1) | P(2) | 84.27(5) | Zr(1) | N(2) | N(2)′ | 67.6(2) |
| Cl(1) | Zr(1) | N(1) | 139.3(1) | Zr(1) | N(2) | Zr(1)′ | 135.1(2) |
| Cl(1) | Zr(1) | N(2) | 112.3(1) | N(2) | Zr(1) | N(2)′ | 44.9(2) |
| Cl(1) | Zr(1) | N(2)′ | 111.9(1) | N(1) | Zr(1) | N(2)′ | 105.5(2) |
| P(1) | Zr(1) | P(2) | 141.00(5) | N(1) | Zr(1) | N(2) | 105.2(1) |
| P(1) | Zr(1) | N(1) | 81.9(1) | P(2) | Zr(1) | N(2)′ | 88.8(1) |
| P(1) | Zr(1) | N(2) | 84.7(1) | P(2) | Zr(1) | N(2) | 133.7(1) |
| P(1) | Zr(1) | N(2)′ | 129.6(1) | P(2) | Zr(1) | N(1) | 80.9(1) |

{[$(Pr^i_2PCH_2SiMe_2)_2N$]Zr($\eta^5$-$C_5H_5$)}$_2(\mu$-$\eta^1$:$\eta^1$-$N_2$) **4a**

| atom | atom | atom | angle | atom | atom | atom | angle |
|---|---|---|---|---|---|---|---|
| P(1) | Zr(1) | P(2) | 145.87(4) | P(3) | Zr(2) | P(4) | 145.65(3) |
| P(1) | Zr(1) | N(1) | 71.74(8) | P(3) | Zr(2) | N(2) | 75.37(7) |
| P(1) | Zr(1) | N(3) | 98.92(8) | P(3) | Zr(2) | N(4) | 86.10(8) |
| P(1) | Zr(1) | Cp(1) | 102.89(6) | P(3) | Zr(2) | Cp(2) | 104.84(6) |
| P(2) | Zr(1) | N(1) | 75.66(8) | P(4) | Zr(2) | N(2) | 71.53(8) |
| P(2) | Zr(1) | N(3) | 85.76(8) | P(4) | Zr(2) | N(4) | 99.76(8) |
| P(2) | Zr(1) | Cp(1) | 104.84(6) | P(4) | Zr(2) | Cp(2) | 102.41(6) |
| N(1) | Zr(1) | N(3) | 115.1(1) | N(2) | Zr(2) | N(4) | 115.3(1) |
| N(1) | Zr(1) | Cp(1) | 127.61(9) | N(2) | Zr(2) | Cp(2) | 127.49(9) |
| N(3) | Zr(1) | Cp(1) | 117.2(1) | N(4) | Zr(2) | Cp(2) | 117.1(1) |
| Zr(1) | N(3) | N(4) | 170.6(2) | Zr(2) | N(4) | N(3) | 170.1(2) |

$SiMe_2)_2N$]ZrCl}$_2(N_2$) (**2a**) in 40% yield; this dinuclear structure

$$ZrCl_3[N(SiMe_2CH_2PR_2)_2] \xrightarrow[1-4\ atm\ N_2]{\text{Na/Hg, 2 - 5 equiv}} \{[(R_2PCH_2SiMe_2)_2N]ZrCl\}_2(N_2) \quad (1)$$

**1a** R = $Pr^i$ (toluene) **2a** R = $Pr^i$

**1b** R = $Bu^t$ **2b** R = $Bu^t$

**1c** R = Me

is consistent with the elemental analysis which shows one $N_2$ unit for two $ZrCl[N(SiMe_2CH_2PPr^i_2)_2]$ units, as well as with mass spectral results and a crystal structure (vide infra). If the reduction is performed in THF or another ether-type solvent, the amount of dinitrogen complex produced is drastically reduced and other as yet unidentified products are formed. Reduction of the related derivative having *tert*-butyl groups at phosphorus, $ZrCl_3[N(SiMe_2CH_2PBu^t_2)_2]$ (**1b**), in the presence of dinitrogen also generates a dinuclear complex of the formula {[$(Bu^t_2PCH_2$-$SiMe_2)_2N$]ZrCl}$_2(N_2$) (**2b**) in similar yields; in this case it was necessary to use sodium sand and longer reduction times (2 weeks) in order to generate green crystals of **2b**. Attempts to reduce the less sterically encumbered material $ZrCl_3[N(SiMe_2CH_2PMe_2)_2]$ (**1c**), having methyl groups at phosphorus, failed to give any tractable material.

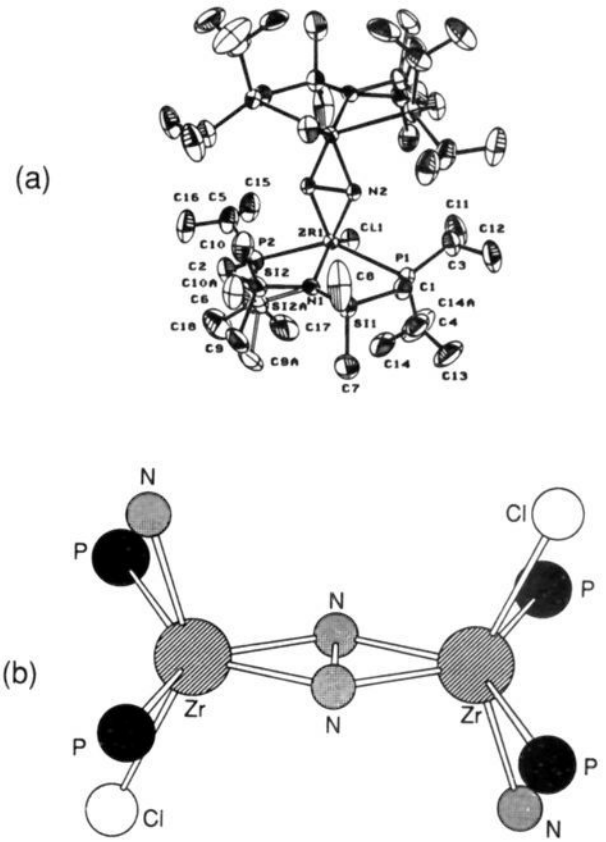


**Figure 1.** (a) Perspective view of **2a**; 25% probability thermal ellipsoids are shown for the non-hydrogen atoms; labeled atoms comprise the asymmetric unit. (b) Inner core of the dimer showing the planar $Zr_2$-($\mu$-$\eta^2$:$\eta^2$-$N_2$) unit (backbone atoms and phosphine substituents removed for clarity).

Although the dinitrogen complex **2a** is only moderately soluble in aromatic solvents, good NMR spectra could be obtained after long accumulation times. The $^{31}P\{^1H\}$ NMR spectrum consists of a singlet at 10 ppm which is temperature invariant from −80 °C to room temperature. On the other hand, the more soluble derivative **2b**, having *tert*-butyl groups at phosphorus, displays an AB quartet in the low-temperature limit (0 °C) which coalesces into a singlet at higher temperatures (25 °C). There are analogous differences in the proton NMR spectra of these complexes: the high-temperature limiting spectrum of **2b** is very similar to the temperature-independent $^1H$ NMR spectrum of **2a** and shows two environments for the silyl ($SiMe_2$), methylene ($PCH_2Si$), and other respective protons; however, at low-temperature **2b**, the derivative having *tert*-butyl substituents shows a pattern typical of a lower symmetry: four silyl methyl and four different *tert*-butyl resonances.

Crystals suitable for X-ray diffraction were obtained only for the isopropyl derivative **2a**, and its solid-state structure was determined. The molecular structure and numbering scheme are shown in Figure 1. The dinuclear structure is immediately apparent as is the fact that there are two $ZrCl[N(SiMe_2CH_2$-$PPr^i_2)_2]$ fragments bridged by a side-on dinitrogen unit. Although there is some disorder in the ligand backbone (see Experimental Section), the planar, symmetric $Zr_2(\mu$-$\eta^2$:$\eta^2$-$N_2)$ core is well determined. The bond lengths from the zirconium to each of the bridging nitrogens (Zr–N(2)) is 2.024(4) Å, and this is shorter than the zirconium–amide bond length (Zr–N(1)) of 2.175(3) Å for the nitrogen donor in the ancillary ligand. Other Zr–N bond distances in the literature range from 1.826(4) Å for a

**Table IV.** Compilation of N–N Bond Lengths for Some Selected Compounds

| compound | bond length (Å) | ref |
|---|---|---|
| $N_2$ | 1.0975(2) | 13 |
| PhN=NPh | 1.255 | 38 |
| $H_2NNH_2$ | 1.46 | 39 |
| $\{[(Pr^i_2PCH_2SiMe_2)_2N]ZrCl\}_2$-$(\mu$-$\eta^2$:$\eta^2$-$N_2)$ **2a** | 1.548(7) | this work |
| $[Cp^*_2Sm]_2(\mu$-$\eta^2$:$\eta^2$-$N_2)$ | 1.088(12) | 22 |
| $[Cp^*_2Zr(N_2)]_2(\mu$-$N_2)$ | 1.182(5) (bridging)<br>1.116(8) (terminal) | 40 |
| $\{[(Pr^i_2PCH_2SiMe_2)_2N]Zr(\eta^5$-$C_5H_5)\}_2(\mu$-$N_2)$ | 1.301(3) | this work |
| $\{[Ph(Na{\cdot}OEt_2)_2]Ph_4Ni_2(\mu$-$N_2)$-$NaLi_6(OEt)_4(Et_2O)\}_2$ | 1.36(2) | 16 |
| $\{(Me_3P)_2(Me_3CCH_2)$-$Ta{=}CHCMe_3\}_2(\mu$-$N_2)$ | 1.298(12) | 41 |
| $\{[(H_3N)_5Ru]_2(\mu$-$N_2)\}^{4+}$ | 1.124(15) | 42 |

zirconium nitrogen double bond[35] in $Cp_2Zr{=}NBu^t(THF)$ to 2.443(1) Å in Schiff base chelate derivatives.[36] The most interesting feature is the very long N–N bond length of 1.548(7) Å in the side-on bridging dinitrogen moiety. This is the longest such bond distance ever reported for a dinitrogen complex and is even longer than that found in hydrazine complexes as well as in $\mu$-$\eta^2$:$\eta^2$-$HNNH^{2-}$ derivatives.[37] As mentioned previously, N–N bond lengths for bridging $N_2$ complexes range from 1.12 to 1.36 Å; a number of examples are given in Table IV.

The geometry around each zirconium in **2a** can be described as distorted square pyramidal if the centroid of the bridging, side-on $N_2$ unit is considered to be occupying the apical site. The two $ZrCl[N(SiMe_2CH_2PPr^i_2)_2]$ fragments quasieclipse each other in the solid-state structure; there is a center of inversion which puts the chloride of one end of the molecule over the amide donor of the other end (see Figure 1).

Apart from the disorder observed, the solution- and solid-state structures of **2a** would appear to correlate quite well. An averaged solution structure with $C_{2h}$ symmetry accounts for both the observed $^1H$ and $^{31}P\{^1H\}$ NMR spectra, particularly the symmetry at high and low temperatures.

Consideration of the possible structures for the *tert*-butyl derivative **2b**, taking into account the differences in spectroscopic behavior in the low-temperature limit, suggests that a similar structure to the isopropyl derivative is possible but that the increased steric bulk does not allow the quasieclipsed structure to be maintained in the low-temperature limit. At low temperatures, a staggered structure may be accessible which renders the phosphorus donors inequivalent and lowers the symmetry of the molecule. Unfortunately, such an analysis does not necessarily imply that the dinitrogen fragment is still bridging side-on since a bridging end-on form could also give rise to the same spectral behavior. In fact there is no definitive evidence for a side-on form in solution for either of the two complexes $\{[(R_2PCH_2$-$SiMe_2)_2N]ZrCl\}_2(\mu$-$N_2)$ (R = $Pr^i$, **2a**, R = $Bu^t$, **2b**).

Attempts to obtain IR and Raman data on these complexes and the $^{15}N_2$-labeled analogues have been inconclusive so far. IR spectra of **2a** and $[^{15}N_2]$**2a** are superimposable with the starting trichloride $ZrCl_3[N(SiMe_2CH_2PPr^i_2)_2]$ (**1a**). Analysis by Raman spectroscopy has been hampered by sample decomposition.

Scheme I

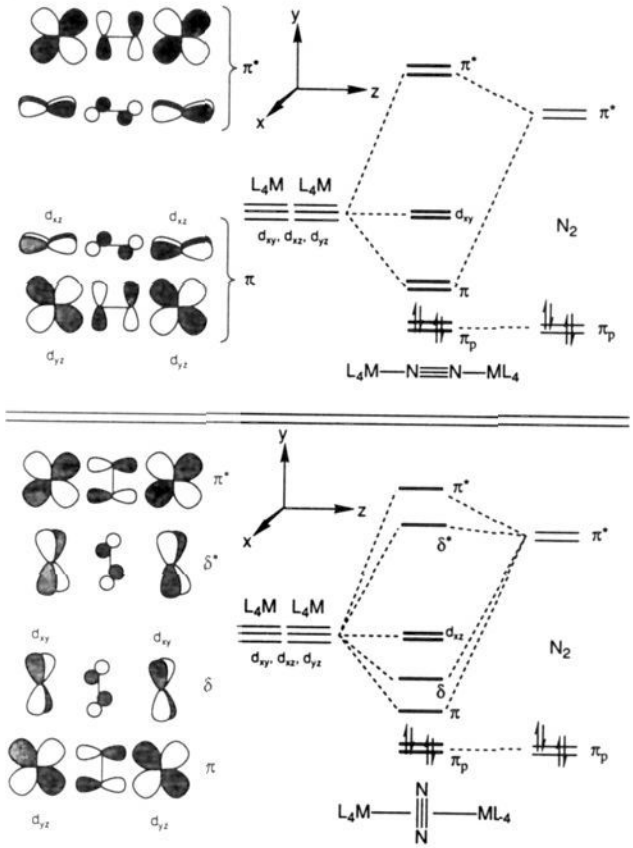


## Bonding Considerations

In an effort to describe the bonding for a side-on structure, it is useful to consider simple qualitative molecular orbital overlap arguments. As mentioned in the Introduction, the experimental evidence for dinitrogen to preferentially bind end-on to transition metals is overwhelming. This can be rationalized qualitatively by the following arguments: the interaction of two $ML_4$ fragments with a single $N_2$ unit can be shown to generate two different types of MO schemes for end-on bridging and side-on bridging, as shown in Scheme I. For simplicity, the $ML_4$ fragments are each considered to have three available d orbitals ($d_{xy}$, $d_{xz}$, and $d_{yz}$) that point between the M–L and $N_2$ ligands;[43] the other two d orbitals ($d_{x^2-y^2}$ and $d_{z^2}$) are used for $\sigma$-bonding with the ligands on the $ML_4$ fragment and with the $N_2$ unit. In the upper part of Scheme I, the analysis for the bridging end-on mode is shown; only the symmetrical interaction with the $\pi^*$-orbitals of the $N_2$ fragment is considered since other calculations of bridging end-on dinitrogen complexes have shown that the overlap of the filled $\pi$-orbitals of the $N_2$ molecule with metal d orbitals is usually quite small.[44] What results from this kind of analysis is that one generates two molecular orbitals in the M–($\mu$-$N_2$)–M fragment with $\pi$-symmetry, which, if occupied, would be bonding for the metal–nitrogen interaction but antibonding with respect to the $N_2$ unit itself. For the analogous side-on analysis shown at the bottom of Scheme I, one generates two bonding molecular orbitals: one molecular orbital has $\pi$-symmetry and the other has $\delta$-symmetry. Once again, both MOs have similar charac-

(35) Walsh, P. J.; Hollander, F. J.; Bergman, R. G. *J. Am. Chem. Soc.* **1988**, *110*, 8729.
(36) Archer, R. D.; Day, R. O.; Illingsworth, M. L. *Inorg. Chem.* **1976**, *18*, 2908.
(37) Blum, L.; Williams, I. D.; Schrock, R. R. *J. Am. Chem. Soc.* **1984**, *106*, 8316.
(38) Allen, F. H.; Kennard, O.; Watson, D. G.; Brammer, L.; Orpen, A. G.; Taylor, R. *J. Chem. Soc., Perkin Trans. II* **1987**, S1.
(39) Sutton, L. E. *Tables of Interatomic Distances and Configuration in Molecules and Ions*; Chemical Society Special Publication No. 11; Chemical Society: London, 1958.
(40) Manriquez, J. M.; Sanner, R. D.; Marsh, R. E.; Bercaw, J. E. *J. Am. Chem. Soc.* **1976**, *98*, 3042.
(41) Turner, H. W.; Fellmann, J. D.; Rocklage, S. M.; Schrock, R. R.; Churchill, M. R.; Wasserman, H. J. *J. Am. Chem. Soc.* **1980**, *102*, 7809.
(42) Treitel, I. M.; Flood, M. T.; Marsh, R. E.; Gray, H. B. *J. Am. Chem. Soc.* **1969**, *91*, 6512.
(43) Albright, T. A.; Burdett, J. K.; Whangbo, M. H. *Orbital Interactions in Chemistry*; Wiley-Interscience: New York, 1985.
(44) Powell, C. B.; Hall, M. B. *Inorg. Chem.* **1984**, *23*, 4619.

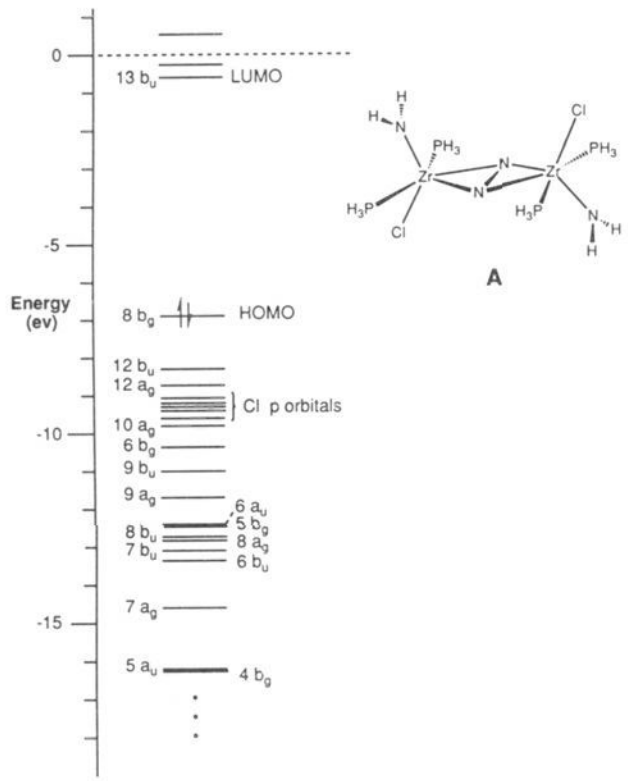


**Figure 2.** INDO/1 semiempirical molecular orbital calculation for **A** using the ZINDO program on a CAChe system.

teristics in that they are bonding with respect to the metal–nitrogen interaction but antibonding for the $N_2$ fragment; however, the main difference is that one would expect the $\delta$-molecular orbital to be less stabilized than the analogous $\pi$-molecular orbital simply on the grounds that the overlap for a $\delta$-bond should be less than for a $\pi$-bond, in analogy to metal–metal quadruple bond arguments.[45] Therefore, the reason that the end-on mode is preferred over the side-on form is simply that the $\delta$-molecular orbital that is formed in the latter mode is not stabilized as much as one of the $\pi$-molecular orbitals; in other words, given the choice between end-on and side-on, the end-on mode is more energetically favored since two $\pi$-orbitals are better than one $\pi$- and one $\delta$-molecular orbital.

It should be noted that for both of the bonding modes in Scheme I, only two of the three available d orbitals from each metal fragment are required, and this, therefore, results in nonbonding d orbitals: for the bridging end-on derivative, two $d_{xy}$ orbitals are unused; for the bridging side-on moiety, two $d_{xz}$ orbitals remain. However, the tacit assumption made even in this simple orbital overlap analysis is that for each metal fragment all three d orbitals are available. What would happen if only two d orbitals per metal fragment were available? In other words, is it possible to force the bridging side-on binding mode because the only two d orbitals available to bind to a bridging $N_2$ unit are those that generate the side-on form?

In an effort to answer these questions, the bonding of the bridging dinitrogen complex **2a** was examined using the INDO/1 semiempirical molecular orbital level of analysis; see Experimental Section for details. To simplify the calculations, the stripped down, symmetrized version of the side-on bound derivative $\{(H_3P)_2Cl(H_2N)Zr\}_2(\mu\text{-}\eta^2\text{:}\eta^2\text{-}N_2)$ (**A**) was used; analogous calculations with the more fully "dressed" backbone having silicons attached to the amide nitrogen as in $\{[(H_2PCH_2SiH_2)_2N]ZrCl\}_2(\mu\text{-}\eta^2\text{:}\eta^2\text{-}N_2)$ gave very nearly identical results. The results of the former calculation are shown in Figure 2.

(45) Cotton, F. A.; Wilkinson, G. *Advanced Inorganic Chemistry*, 5th ed.; Wiley-Interscience: New York, 1988; p 1085.

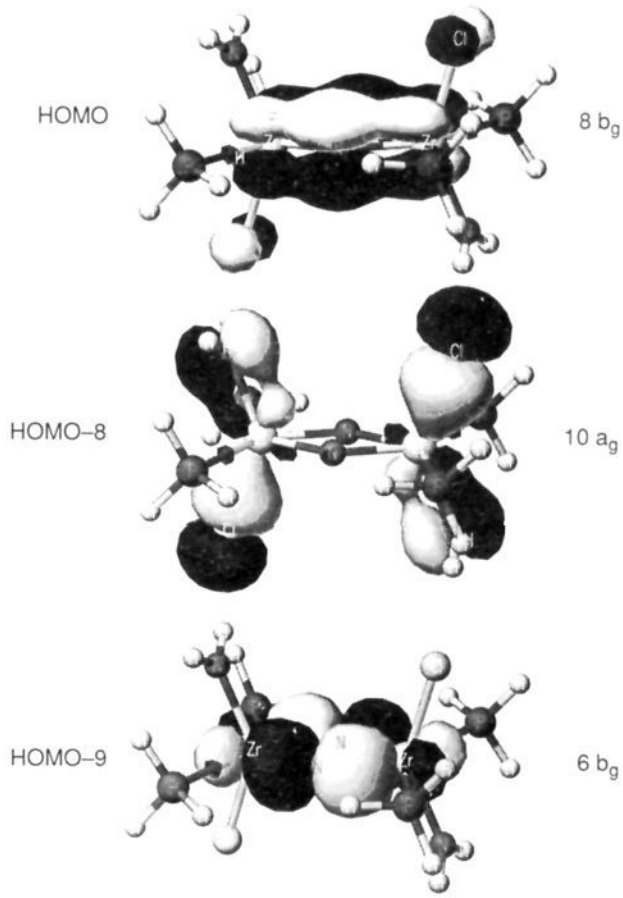


**Figure 3.** Isosurface plots for the indicated levels of the ZINDO calculation for the model compound $\{(H_3P)_2Cl(H_2N)Zr\}_2(\mu\text{-}\eta^2\text{:}\eta^2\text{-}N_2)$ **A** for $\Psi$ = 0.03 au (dark grey area = $+\Psi$; light grey area = $-\Psi$).

The molecular orbitals of interest are the HOMO, HOMO-9, and HOMO-8; these are shown in Figure 3. The HOMO (8 $b_g$) is at –6.937 eV and is the $\delta$-molecular orbital; HOMO-9 (6 $b_g$) is the $\pi$-molecular orbital and is at –10.329 eV; both of these orbitals are essentially identical to that predicted by the qualitative analysis summarized in Scheme I. Another important molecular orbital is HOMO-8 (10 $a_g$) at –9.779 eV, since this shows that one of the d orbitals is somewhat involved in $\pi$-bonding with the amide lone pair, in addition, there is a strong Zr–Cl $\sigma$-interaction. This analysis of the bridging side-on bound dinitrogen product **A** suggests that there are only two d orbitals available on each Zr fragment for bonding with the dinitrogen ligand (excluding $\sigma$-bonding orbitals). Therefore, it is the amide donor of the tridentate ligand which prevents the formation of the typical end-on bridging form because it is held by the phosphine ligands in such a conformation that it overlaps with the appropriate d orbital to form a $\pi$-bond in lieu of a $\pi$-bond with the end-on $N_2$; the $\sigma$-interaction with the chloride is undoubtedly also important.

### Fragment Orbital Analysis

In an effort to isolate the effect of the ancillary ligand arrangement, the frontier orbitals of the fragment ends of the dinuclear dinitrogen derivative were examined. The analysis was performed on the symmetrized moiety *trans*-$ZrCl(NH_2)(PH_3)_2$ (**B**), in which the metal was raised out of the coordination plane of the donors by 20° to duplicate the geometry of the dinitrogen complex **2a**; this is shown in Scheme II. Since it is suggested that orientation of the amide donor is partly responsible for the occurrence of the side-on mode, the effect of rotating the $NH_2^-$ donor was also examined. Qualitatively, it seems intuitive that upon rotation of the $NH_2$ unit by 90°, the lone pair in the p

**Scheme II**

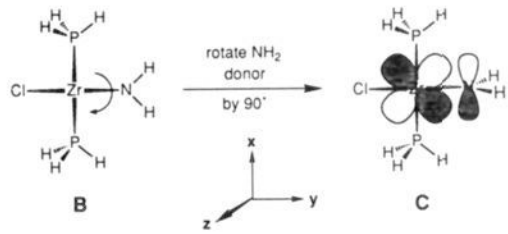


**Scheme III**

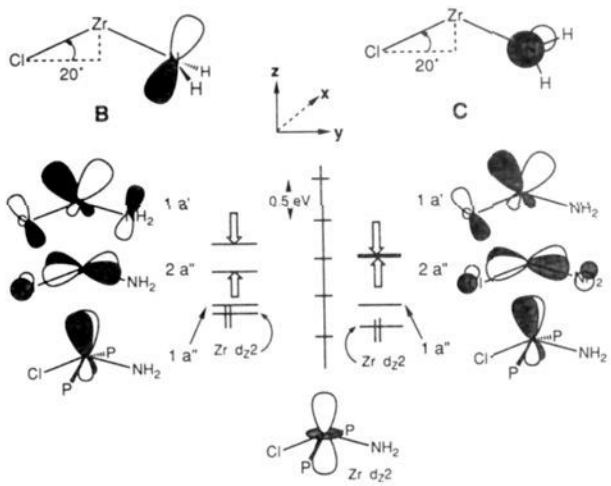


orbital on the amide nitrogen would now be set up to overlap with the $d_{xy}$ orbital, thereby rendering it less available for overlap with the $\pi^*$-orbital on the $N_2$ fragment to form the $\delta$-molecular orbital; in other words, rotation of the amide donor to generate the conformational isomer **C** should tend to disfavor the side-on form.

A slightly more rigorous analysis is shown in Scheme III; the frontier orbitals of the fragment **B** are shown, as are those of the conformer **C**, having the $NH_2^-$ rotated by 90°. In both **B** and **C** the $d_{z^2}$ is the HOMO. In **B**, the frontier orbitals clearly show that the two a″ orbitals have the correct symmetry to generate the observed $\pi$- and $\delta$-molecular orbitals for the side-on structure. The 1a′ orbital of **B** is the highest in energy because it is the antibonding counterpart of the bonding molecular orbital in which the p orbital of the amide nitrogen (and a p orbital on the chloride, to some extent) overlaps with that d orbital that would have been used to form the second $\pi$-bond of the end-on form; the energy gap between these two frontier orbitals is calculated to be 37 kJ mol$^{-1}$. In conformer **C**, the effect of rotating the amide can be seen in the relative energies of the frontier orbitals; in this case the 1a′ and 2a″ are now nearly degenerate ($\Delta E$ = 0.5 kJ mol$^{-1}$) since the 1a′ orbital in **C** is lowered relative to that in **B**, while the 2a″ orbital is correspondingly raised because the bonding counterparts of these antibonding frontier orbitals are destabilized and stabilized, respectively, due to changes in the overlap with the p orbital of the amide nitrogen. This suggests that the end-on mode should be preferred for **C** since we now have the situation described earlier in Scheme I, that is, if given the choice, the end-on mode of binding should be preferred because of overlap arguments for $\pi$- versus $\delta$-molecular orbitals. Support for this analysis can be found in two recent X-ray structures of related isoelectronic dinuclear titanium dinitrogen complexes, shown in **D1** and **D2** below, both of which display the bridging end-on mode.[18,46] In **D1**, having cis-disposed neutral amine donors rather than trans-disposed phosphine ligands (as in **2a**), the major difference is that the bis(trimethylsilyl)amide ancillary ligand is

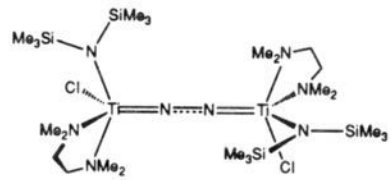

**D1**

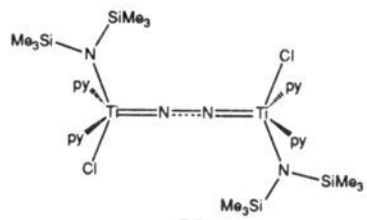

**D2**

arranged perpendicular to the plane defined by the donor atoms; this is also found in **D2**, but now the neutral pyridine donors are trans-disposed. Both of these complexes are similar to that proposed in conformer **C**, and their structures are a reasonable consequence of the fact that both **D1** and **D2** have no conformational restrictions to force the amide ligand to bond in a manner as is found in the chelating amido–diphosphine ligand of the side-on derivative **2a**.

### Other Dinitrogen Complexes

The analysis given above prompted us to examine the effect of changing the ligand environment. Clearly, the amide donor of the ancillary ligand is important, but just how important is the chloride moiety? The reaction of the starting trichloride derivative $ZrCl_3[N(SiMe_2CH_2PPr^i_2)_2]$ (**1a**) with sodium cyclopentadienide generates the cyclopentadienyl complex **3a** ($Zr(\eta^5\text{-}C_5H_5)Cl_2[N(SiMe_2CH_2PPr^i_2)_2]$). From the solution spectroscopic data, the structure of this derivative has the cyclopentadienyl unit trans to the amide donor in a quasioctahedral array; this has been confirmed by a single-crystal X-ray study of the related dibromo derivative $Zr(\eta^5\text{-}C_5H_5)Br_2[N(SiMe_2CH_2PPr^i_2)_2]$.[47] Reduction of this modified complex under dinitrogen generates the dinuclear dinitrogen complex $\{[(Pr^i_2PCH_2SiMe_2)_2N]Zr(\eta^5\text{-}C_5H_5)\}_2(\mu\text{-}N_2)$ (**4a**) as dark brown crystals; this is summarized in Scheme IV. In solution, the spectroscopic behavior of this particular dinitrogen-containing species is straightforward and mirrors the *tert*-butyl derivative $\{[(Bu^t_2PCH_2SiMe_2)_2N]ZrCl\}_2(\mu\text{-}N_2)$ (**2b**); in the high-temperature limit, the phosphine donors give rise to a singlet in the $^{31}P\{^1H\}$ NMR spectrum which upon cooling decoalesces into an AB quartet with $^2J_{P\text{-}P}$ = 80 Hz. In this case, suitable crystals of **4a** were obtained for an X-ray study.

The molecular structure of the cyclopentadienyl-containing dinitrogen complex is shown in Figure 4. In this case the dinitrogen unit is bridging end-on; the N–N bond distance is 1.301(3) Å, much shorter than that observed for the side-on complex discussed above. The Zr–N bond lengths of **4a** are significantly different from that found in the side-on complex **2a**: the distances to the $N_2$ are 1.920(3) and 1.923(3) Å, respectively, for Zr(1)–N(3) and Zr(2)–N(4), shorter by 0.1 Å than those in the side-on derivative; the zirconium–amide lengths of **4a** are correspondingly longer than that of **2a** by approximately 0.1 Å (i.e., Zr(1)–N(1), Zr(2)–N(2) at 2.306(3) and 2.303(3) Å, respectively). The molecule has $C_2$ symmetry in the solid state; each $Zr(\eta^5\text{-}C_5H_5)[N(SiMe_2CH_2PPr^i_2)_2]$ unit has the tridentate ligand twisted in such a way that one phosphorus donor is closer to the cyclopentadienyl unit than the other. In solution, this type of structure would account for the inequivalent phosphorus nuclei found in the low-temperature limit. At higher temperatures,

(46) Beydoun, N.; Duchateau, R.; Gambarotta, S. *J. Chem. Soc., Chem. Commun.* **1992**, 244.

(47) Fryzuk, M. D.; Mylvaganam, M.; Rettig, S. J., unpublished results.

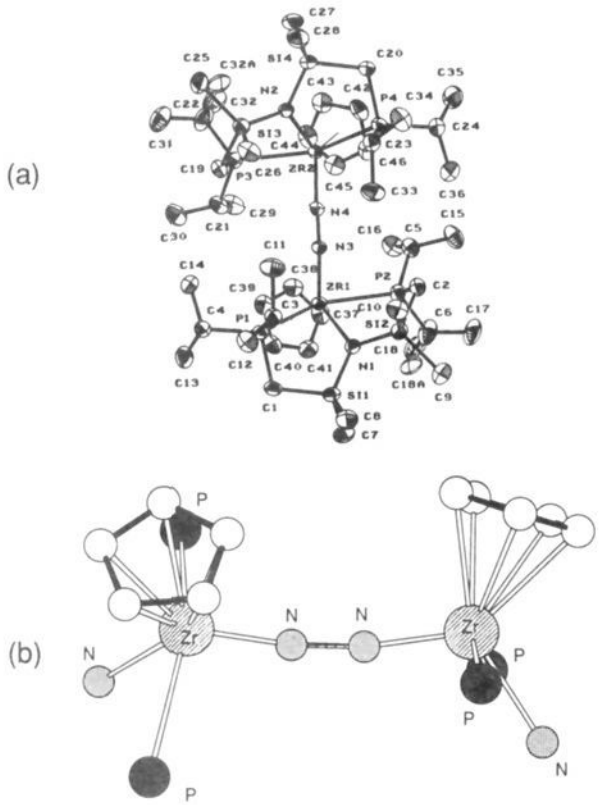


**Figure 4.** (a) Perspective view of **4a**; 33% probability thermal ellipsoids are shown for the non-hydrogen atoms. (b) Inner core of the dimer showing the end-on structure of the bridging $N_2$ unit (backbone atoms and phosphine substituents removed for clarity).

**Scheme IV**

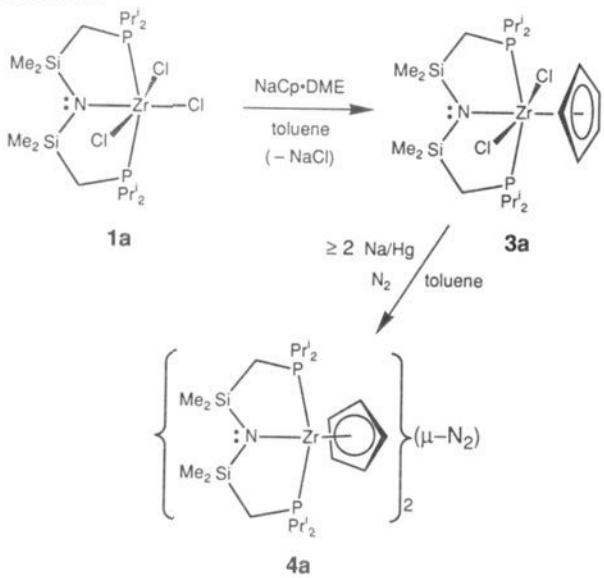


some process equilibrates the two phosphorus donors, perhaps via pivoting of the $NSi_2$ plane and movement of the cyclopentadienyl unit, or alternatively, by phosphine dissociation.

How can one rationalize the end-on bonding of the dinitrogen in this dinuclear complex? Basically what has happened is that the replacement of the chloride ligand by a cyclopentadienyl group has altered the available d orbitals. Analysis of the molecular orbitals of the fragment *trans*-$Zr(\eta^5\text{-}C_5H_5)NH_2(PH_3)_2$ shows that the d orbital that would be used to generate the $\delta$-molecular orbital for a side-on $N_2$ fragment overlaps with the $\pi$-orbitals of the cyclopentadienyl ligand. This is schematically shown in **E**.

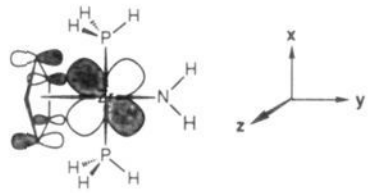


**E**

A further point concerns the two $\pi$-molecular orbitals that form with the $N_2$ fragment for this end-on bridging mode; given our earlier analysis, there should be no overlap of the p orbital on the amide of the ancillary ligand with the appropriate d orbital, since this d orbital will be involved in a $\pi$-interaction with $N_2$ ligand. That this is the case in this complex can be seen by the lengthening of the zirconium–amide (Zr–N(1) and Zr–N(2)) bonds in the dinitrogen complex **4a** as compared to the side-on derivative **2a**. In fact, the zirconium–amide bond distances in **4a** (2.306(3) and 2.303(3) Å) are the longest of any Zr–N bond lengths that we have measured for this ligand system coordinated to Zr[24,48,49] and are just slightly shorter than the distances of 2.443(1) and 2.412(2) Å found in neutral amine-type adducts of Zr(IV).[36,50] It is noteworthy that in the solid-state structure the $NSi_2$ plane in the tridentate ligand is twisted with respect to the plane of the three donors ($NP_2$), and this would be expected to further minimize overlap between the lone pair on the amide and any available d orbital.

The preparation of this end-on bridging $N_2$ complex **4a** could also be achieved by reaction of the side-on complex **2a** with NaCp·DME in THF as shown in eq 2. Thus, displacement of

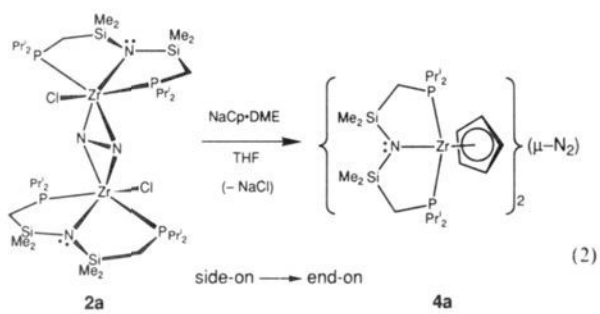


(2)

the chloride by the cyclopentadienyl unit results in the isomerization of the dinitrogen unit from side-on to end-on since the isolated dinuclear cyclopentadienyl derivative **4a** is identical in all respects to that formed by reduction of the dichloride **3a**. When this reaction was performed with the nitrogen-15-labeled material $\{[(Pr^i_2PCH_2SiMe_2)_2N]ZrCl\}_2(\mu\text{-}\eta^2\text{:}\eta^2\text{-}^{15}N_2)$ under an atmosphere of unlabeled dinitrogen ($^{14}N_2$), no incorporation of unlabeled $N_2$ label was found in the product as measured by mass spectroscopy; in other words, the metathesis of the chloride does not involve any process whereby exchange between coordinated $N_2$ and free $N_2$ is kinetically significant.

So far, only electronic effects in the analysis of side-on versus end-on dinitrogen binding have been examined. What about steric considerations? All of the complexes so far examined are dinuclear, and steric aspects should be important since the end-on bridging mode obviously keeps the ends of these molecules further apart than the side-on bridging mode; in fact, in the side-on derivative **2a** the separation between the two Zr centers is 3.7 Å, whereas in the cyclopentadienyl complex **4a** the zirconium–zirconium distance is 5.1 Å. One could argue that the reason the

(48) Fryzuk, M. D.; Haddad, T. S.; Rettig, S. J. *Organometallics* **1989**, *8*, 1723.
(49) Fryzuk, M. D.; Rettig, S. J.; Williams, H. D. *Inorg. Chem.* **1983**, *22*, 863.
(50) Peterson, E. J.; von Dreele, R. B.; Brown, T. M. *Inorg. Chem.* **1976**, *15*, 309.

cyclopentadienyl derivative **4a** displays the end-on dinitrogen bonding mode is purely steric in origin because the cyclopentadienyl group in **4a** is bulkier than the chloride ligand in **2a** and thus the side-on bridging mode is destabilized. One way that we have examined to try to get around this is to move to group 5 analogues. The tantalum neopentylidene and benzylidene derivatives, $Ta{=}CHR(Cl)_2[N(SiMe_2CH_2PPr^i_2)_2]$ (R = Bu$^t$, **5**; R = Ph, **6**) containing the identical tridentate ancillary ligand were reduced under $N_2$ to generate the dinuclear dinitrogen complexes $\{[(Pr^i_2PCH_2SiMe_2)_2N]Ta{=}CHR\}_2(\mu\text{-}N_2)$ (R = Bu$^t$, **7**; R = Ph, **8**); although no suitable crystals for X-ray analysis could be

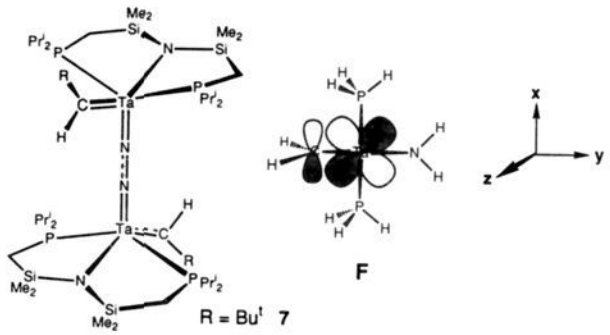


obtained, both of these complexes are assumed to have the dinitrogen bound in an end-on, bridging mode in analogy to that found in the related derivatives $\{(Me_3P)_2ClTa{=}CHBu^t\}_2(\mu\text{-}N_2)$[51] and $\{(Me_3P)_2(CH_2Bu^t)Ta{=}CHBu^t\}_2(\mu\text{-}N_2)$.[41,52]

In this case, upon replacement of the chloride with a neopentylidene group (and Ta for Zr), one can rationalize the bridging end-on form as due to overlap of the p orbital of the alkylidene unit with that particular d orbital that would have otherwise engaged in $\delta$-bonding with the side-on dinitrogen fragment, as shown in **F**. Indeed, the frontier orbitals of **F** show an orbital ordering slightly different from that of either of the zirconium fragments **B** or **C** (see Scheme III) since now the 2a″ orbital is considerably higher in energy than the 1a′, thus generating frontier orbitals with the correct symmetry to generate the end-on binding mode.

## $^{15}$N NMR Chemical Shifts

In Table V are shown some $^{15}$N NMR chemical shifts of a series of selected dinitrogen complexes. Originally, we had hoped that measurement of the $^{15}$N chemical shift would provide a diagnostic handle on the mode of binding in these derivatives, that is, side-on bridging versus end-on bridging. However, as is evident from the chemical shifts in Table V, there is no obvious correlation. For example, the chemical shift of the side-on complex **2a**, whether in the solid form or in solution, is in the range of 345–351 ppm, while the end-on derivative **4a** is at 354 ppm. In fact, the only correlation seems to be to which metal the dinitrogen ligand is attached, since the zirconium complexes resonate around 350 ppm with the exception of the bridging $N_2$ of $[Cp^*_2Zr(N_2)]_2(\mu\text{-}N_2)$. The dinuclear tantalum complexes also display very similar chemical shifts irrespective of the ancillary ligands; also notable is that the formally W(VI) derivative $[Cp^*WMe_3]_2(\mu\text{-}N_2)$ and the mononuclear Mo(0) complex *trans*-$Mo(N_2)_2(PMePh_2)_4$ both show chemical shifts similar to those of these tantalum dinitrogen complexes.

**Table V.** Compilation of $^{15}$N Chemical Shifts[a] for Some Selected Compounds

| compound | chemical shift (ppm) | ref |
|---|---|---|
| $\{[(Pr^i_2PCH_2SiMe_2)_2N]ZrCl\}_2(\mu\text{-}\eta^2{:}\eta^2\text{-}N_2)$ **2a** | 350.9 (solution)<br>345.0 (solid) | this work |
| $\{[(Pr^i_2PCH_2SiMe_2)_2N]Zr(\eta^5\text{-}C_5H_5)\}_2(\mu\text{-}N_2)$ **4a** | 354.0 | this work |
| $[Cp^*_2Zr(N_2)]_2(\mu\text{-}N_2)$ | 452.0[b] (bridging)<br>354.0[b] (terminal) | 53 |
| $\{[(Pr^i_2PCH_2SiMe_2)_2N]\text{-}Ta{=}CHBu^t\}_2(\mu\text{-}N_2)$ **7** | 301.2 | this work |
| $\{(Me_3P)_2ClTa{=}CHCMe_3\}_2(\mu\text{-}N_2)$ | 296.2[c] | 51 |
| $[Cp^*WMe_3]_2(\mu\text{-}N_2)$ | 310.9[c] | 54 |
| *trans*-$Mo(N_2)_2(PMePh_2)_4$ | 305.4[d] | 55 |

[a] All chemical shifts are referenced to external neat formamide set at 0.0 ppm. [b] Originally referenced to nitric acid. [c] Originally referenced to liquid ammonia. [d] Originally referenced to nitromethane.

## Hydrazine Analysis

Both the side-on bridged dinitrogen complex of zirconium **2a** and the related end-on derivative **4a** react with excess gaseous HCl to release 1 equiv of hydrazine per respective dinuclear complex as analyzed by colorimetry.[28] This stoichiometric reaction is accompanied by complete decomposition of the zirconium-containing side products, presumably due to the sensitive nature of the N–Si linkage in the ancillary ligand backbone.

## Conclusion

The factors which control the side-on versus end-on bridging forms of dinitrogen have been investigated both by synthetic studies and by molecular orbital analysis. What arises from this work is that the ancillary ligands are paramount in determining which of the two possible bonding modes is found. This appears to be a matter of selecting two of the three available d orbitals on a metal fragment to favor one or the other mode of bonding. While this analysis is somewhat simplified, it does provide a framework for the design of other side-on bound dinitrogen complexes.

One of the most interesting aspects of the side-on derivative **2a** is the observed long N–N bond length in the solid-state structure. A bond distance of 1.548(7) Å is significantly longer than the prototypical N–N single bond of hydrazine reported at 1.46 Å. Yet in end-on complexes, for example as found in the dinuclear cyclopentadienyl derivative **4a**, the bond length is more typically 1.30 Å. Why is there such a huge difference between the side-on and the end-on modes? As already discussed in Scheme I, both the $\pi$- and the $\delta$-molecular orbitals of the side-on form are antibonding with respect to the N–N unit, but this is also true for the bonding $\pi$-molecular orbitals of the bridging end-on derivative. The difference may well be that the $\pi$-molecular orbital of the side-on form is so low in energy that it contributes more to the bond order than similar $\pi$-orbitals of the end-on form. Since these orbitals are antibonding with respect to the N–N fragment, the more stable the orbital, the longer the N–N bond distance. In fact, if one considers formal oxidation states of the two dinuclear zirconium complexes reported here, both **2a** and **4a** have Zr(IV) centers with a bridging $N_2^{4-}$ unit; while such an analysis is simplistic, one cannot but arrive at the conclusion that it is not that the side-on form has such a long N–N bond length, but rather that the end-on form has anomalously short bond distances. Interestingly, upon acidification both the side-on complex **2a** and the end-on derivative **4a** generate 1 equiv of hydrazine, as would be predicted from two Zr(IV) fragments bound to a hydrazido(4-) unit.

(51) Rocklage, S. M.; Turner, H. W.; Fellmann, J. D.; Schrock, R. R. *Organometallics* **1982**, *1*, 703.
(52) Churchill, M. R.; Wasserman, H. J. *Inorg. Chem.* **1981**, *20*, 2899.
(53) Manriquez, J. M.; McAlister, D. R.; Rosenberg, E.; Shiller, A. M.; Williamson, K. L.; Chan, S. I.; Bercaw, J. E. *J. Am. Chem. Soc.* **1978**, *100*, 3078.
(54) O'Regan, M. B.; Liu, A. H.; Finch, W. C.; Shrock, R. R.; Davis, W. M. *J. Am. Chem. Soc.* **1990**, *112*, 4331.
(55) Lazarowych, N. J.; Morris, R. H.; Ressner, J. M. *Inorg. Chem.* **1986**, *25*, 3926.

In the side-on bound dinitrogen complex **2a**, the HOMO was shown to be of $\delta$-symmetry. The occurrence of $\delta$-bonds is rather rare and is so far entirely confined to inorganic chemistry. The classic example of $\delta$-bonds in metal–metal quadruple bonds is probably the most well known,[45] although there are other examples of molecular orbitals with this symmetry.[56] In the case of the side-on dinitrogen complexes, it turns out that the existence of a $\delta$-molecular orbital is probably not critical to the stabilization of this particular binding mode, since there are ab initio theoretical studies[57] on mononuclear bis(phosphine)nickel dinitrogen complexes which conclude that the side-on mode is preferred over the end-on structure without invoking a $\delta$-molecular orbital; in fact, for $(H_3P)_2Ni(\eta^2\text{-}N_2)$, it is the $\pi$-orbital which is suggested to be most important.

(56) Thorn, D. L.; Nugent, W. A.; Harlow, R. L. *J. Am. Chem. Soc.* **1981**, *103*, 357.
(57) Rosi, M.; Sgamellotti, A.; Tarantelli, F.; Floriani, C.; Cederbaum, L. S. *J. Chem. Soc., Dalton Trans.* **1989**, 33.

Studies are continuing in our laboratory to further probe the effects of both the ligands and the metal on the mode of bonding of the dinitrogen molecule. We are also interested in the reactivity patterns of side-on versus end-on dinitrogen ligands.

**Acknowledgment.** This work was supported by the NSERC of Canada. We also thank Professor Thomas M. Loehr for discussions.

**Supplementary Material Available:** Details of the molecular orbital calculations including parameters used and Cartesian coordinates for all the models; final atomic coordinates and equivalent isotropic thermal parameters, hydrogen atom parameters, anisotropic thermal parameters, complete tables of bond lengths and bond angles, torsion angles, intermolecular contacts, and least-squares planes for **2a** and **4a** (62 pages); observed and calculated structure factor amplitudes for **2a** and **4a** (77 pages). Ordering information is given on any current masthead page.